JCI The Journal of Clinical Investigation

mTORC1 feedback to AKT modulates lysosomal biogenesis through MiT/TFE regulation

Kaushal Asrani, … , Michael Skaro, Tamara L. Lotan

J Clin Invest. 2019. https://doi.org/10.1172/JCI128287.

Research In-Press Preview **Metabolism** **Oncology**

The Microphthalmia family of transcription factors (MiT/TFE) controls lysosomal biogenesis and is negatively regulated by the nutrient sensor mTORC1. However, the mechanisms by which cells with constitutive mTORC1 signaling maintain lysosomal catabolism remain to be elucidated. Using the murine epidermis as a model system, we found that epidermal *Tsc1* deletion resulted in a phenotype characterized by wavy hair and curly whiskers, and was associated with increased EGFR and HER2 degradation. Unexpectedly, constitutive mTORC1 activation with *Tsc1* loss increased lysosomal content via up-regulated expression and activity of MiT/TFEs, while genetic deletion of *Rheb* or *Rptor* or prolonged pharmacologic mTORC1 inactivation had the reverse effect. This paradoxical increase in lysosomal biogenesis by mTORC1 was mediated by feedback inhibition of AKT, and a resulting suppression of AKT-induced MiT/TFE down-regulation. Thus, inhibiting hyperactive AKT signaling in the context of mTORC1 loss-of-function fully restored MiT/TFE expression and activity. These data suggest that signaling feedback loops work to restrain or maintain cellular lysosomal content during chronically inhibited or constitutively active mTORC1 signaling respectively, and reveal a mechanism by which mTORC1 regulates upstream receptor tyrosine kinase signaling.

Find the latest version:

https://jci.me/128287/pdf

mTORC1 feedback to AKT modulates lysosomal biogenesis through MiT/TFE regulation

Authors: Kaushal Asrani[1,*], Sanjana Murali[1], Brandon Lam[1], Chan-Hyun Na[2], Pornima Phatak[3], Akshay Sood[1], Harsimar Kaur[1], Zoya Khan[1], Michaël Noë[1], Ravi K Anchoori[1], C. Conover Talbot Jr[4], Barbara Smith[5], Michael Skaro[1], Tamara L. Lotan[1,*]

Affiliations:

[1]Department of Pathology, Johns Hopkins University School of Medicine, Baltimore, MD 21231, USA.

[2]Institute for Cell Engineering; Johns Hopkins University School of Medicine, Baltimore, MD 21231, USA.

[3]Baltimore Veteran Affairs Medical Center, Baltimore, MD 21201, USA.

[4]Institute for Basic Biomedical Sciences; Johns Hopkins University School of Medicine, Baltimore, MD 21231, USA.

[5]Department of Cell Biology, Johns Hopkins University School of Medicine, Baltimore, MD 21231, USA.

[*]Correspondence should be addressed to**:**

Tamara Lotan, MD or Kaushal Asrani MBBS, PhD
1550 Orleans Street
Baltimore, MD 21231
(410) 614-9196 (ph)
e-mail: tlotan1@jhmi.edu
kasrani1@jhmi.edu

Abstract: The Microphthalmia family of transcription factors (MiT/TFE) controls lysosomal biogenesis and is negatively regulated by the nutrient sensor mTORC1. However, the mechanisms by which cells with constitutive mTORC1 signaling maintain lysosomal catabolism remain to be elucidated. Using the murine epidermis as a model system, we found that epidermal *Tsc1* deletion resulted in a phenotype characterized by wavy hair and curly whiskers, and was associated with increased EGFR and HER2 degradation. Unexpectedly, constitutive mTORC1 activation with *Tsc1* loss increased lysosomal content via up-regulated expression and activity of MiT/TFEs, while genetic deletion of *Rheb* or *Rptor* or prolonged pharmacologic mTORC1 inactivation had the reverse effect. This paradoxical increase in lysosomal biogenesis by mTORC1 was mediated by feedback inhibition of AKT, and a resulting suppression of AKT-induced MiT/TFE down-regulation. Thus, inhibiting hyperactive AKT signaling in the context of mTORC1 loss-of-function fully restored MiT/TFE expression and activity. These data suggest that signaling feedback loops work to restrain or maintain cellular lysosomal content during chronically inhibited or constitutively active mTORC1 signaling respectively, and reveal a mechanism by which mTORC1 regulates upstream receptor tyrosine kinase signaling.

Keywords: mTORC1, MiT/TFE, EGFR, Lysosome, AKT, TSC, HER2, Torin, Raptor, Epidermis

Introduction

The Microphthalmia family of transcription factors (MiT/TFE) is composed of four conserved members (*Mitf*/*Tfe3*/*Tfeb*/*Tfec*) that are essential regulators of lysosomal biogenesis and autophagy. MiTs are functionally redundant and regulate transcription at CLEAR (coordinated lysosomal expression and regulation) motifs on lysosomal/autophagy target genes. The regulation of MiT/TFE transcriptional activity is complex and understood to be governed by short-term subcellular localization changes driven principally by mTORC1 kinase signaling (1). According to current models, phosphorylation of MiT/TFE proteins by mTORC1 leads to their cytoplasmic retention, resulting in decreased lysosomal biogenesis (2-6). This is consistent with the known role of mTORC1, a key sensor of cellular nutrient levels, in the negative regulation of autophagy (7).

However, this model of MiT/TFE regulation raises an important question: how can cells maintain lysosomal content in the face of persistent mTORC1 signaling? Up-regulated mTORC1 activity and lysosomal biogenesis must co-exist during physiological states like recovery from starvation (8) and physical exercise (9, 10). Strikingly, several lines of evidence suggest that constitutive/prolonged mTORC1 activity may itself paradoxically *activate* lysosomal biogenesis via increased MiT/TFE activity. In a small number of studies, constitutive mTORC1 hyperactivity (via *Tsc1/2* loss) *positively* regulated TFEB-dependent lysosomal genes (11) and *promoted* TFE3 nuclear localization in an mTORC1-dependent manner (12, 13), through undefined mechanisms. Furthermore, MiT/TFEs themselves stimulate mTORC1 activity in multiple cell types in response to nutrients, though their effect on cells with constitutive mTORC1 activation is less certain (14). These findings suggest the intriguing possibility of an mTORC1-MiT/TFE positive feedback loop. Notably, MiT/TFE activity is also co-regulated by numerous oncogenic pathways in parallel to mTORC1, including ERK, GSK3, PKC and AKT (15-17). Taken together, these data raise the

likelihood that mTORC1 regulation of MiT/TFE activity is more complex than previously appreciated.

As a first step to understanding how mTORC1 regulates MiT/TFE activity, we studied isogenic normal cells with or without genetic perturbations leading to constitutive or abrogated mTORC1 signaling. The epidermis and primary keratinocyte cultures provide a unique and well-characterized epithelial model system where the lysosome plays an important role in cellular differentiation and homeostasis (18), thus we developed genetically engineered mouse models of *Tsc1, Rheb* or *Rptor* conditional deletion in the epidermis. Herein, we demonstrate that in the context of long-term, bi-directional mTORC1 signaling perturbation, mTORC1 feedback to AKT prevails to regulate MiT/TFE levels and lysosomal biogenesis. These findings begin to explain how constitutive mTORC1 activation may up-regulate lysosomal catabolism and provide a mechanism by which mTORC1 signaling feedback modulates upstream EGFR and HER2 activity.

Results

Epidermal mTORC1 gain-of-function models have skin defects reminiscent of epidermal EGFR or TGFα loss.

Germline inactivation of *Tsc1* is associated with embryonic lethality (19). To study mTORC1 function in the epidermis, we examined mice with conditional deletion of epidermal *Tsc1* by crossing floxed *Tsc1* mice (*Tsc1* $^{flox/flox}$) with *Krt14-Cre* mice (which express Cre recombinase driven by the keratin 14 promoter in the basal epidermis by E14.5), to generate *Tsc1* $^{flox/flox}$ /*Krt14-Cre* mice (*Tsc1* cKO). The presence of *Tsc1* $^{flox/flox}$ alleles and *Krt14-Cre* was confirmed by PCR genotyping (**Figure 1A**). TSC1 loss was verified by immunoblots from epidermal lysates (**Figure 1B**). In addition, we also prepared parallel primary keratinocyte cultures from these mice to further allow *in vitro* perturbation experiments in this system and confirm all *in vivo* findings (**Figure 1B**). *Tsc1* cKO mice were viable and born in the expected Mendelian ratios. However, they could be distinguished by curly vibrissae at birth and coarse, wavy fur by 4 weeks (**Figure 1C**). During this period, *Tsc1* cKO mice developed epidermal thickening and showed increased p-S6 levels by immunofluorescence, consistent with increased mTORC1 activity (**Figure 1D**). By 6 months, *Tsc1* cKO mice had hair loss and severe facial inflammation (**Figure 1E**), a phenotype strikingly similar to murine epidermal TGF-α or EGFR loss (20-22). To verify mTORC1-dependency of this phenotype, we crossed *K14*-cre mice with *Rheb S16H* $^{flox/flox}$ mice, which express a constitutively active *Rheb* transgene resistant to TSC GAP activity expressed upon Cre excision of a *loxp-stop-loxp* (23). Genotyping PCR confirmed the presence of *S16H* $^{flox/flox}$ alleles, *S16H* excision alleles and *Krt14-Cre* in *Rheb S16H* transgenic (Tg) mice (**Figure 1F**). mTORC1 hyperactivity was confirmed by increased p-S6 levels by epidermal immunofluorescence and keratinocyte

immunoblotting (**Figures 1G and S1A**). These mice also had wavy fur (**Figure 1H**), confirming that the *Tsc1* cKO phenotype was due to increased *Rheb*/mTORC1 activity.

mTORC1 hyperactivation in Tsc1 cKO epidermis and keratinocytes downregulates EGFR and HER2 protein expression and activity

To assess whether the epidermal phenotype in *Tsc1* cKO mice was due to a dysfunction in the EGF pathway, we examined expression of EGFR and its principal binding partner HER2. EGFR and HER2 protein expression were significantly decreased in postnatal day 7 (P7) *Tsc1* cKO epidermal lysates (**Figure 2A**) and keratinocytes (**Figure 2B**) and in *Tsc1* $^{flox/flox}$ keratinocytes infected with adenovirus expressing cre recombinase (*Tsc1* cre), compared to their respective controls, by immunoblotting (**Figure 2C**). Within the TSC1-TSC2 complex, TSC1 stabilizes TSC2, while TSC2 acts as a GTPase-activating protein (GAP) for Rheb and together the complex modulates mTORC1 activity. TSC2 expression in *Tsc1* cKO epidermal lysates was decreased (**figure S1B**) as previously described (24). In addition, there was decreased EGFR and HER2 protein expression in *Tsc2* $^{flox/flox}$ keratinocytes infected with adenoviral cre (**figure S1C**). Membrane localized EGFR and HER2 in *Tsc1* cKO keratinocytes was also decreased, by surface biotinylation assays (**Figure 2D**). mTORC1 hyperactivity in *Tsc1* cKO keratinocytes was confirmed by increased p-S6 levels by immunoblotting, and mTORC1 inhibition using rapamycin or mTOR kinase inhibitors AZD8055 or Torin1 increased EGFR and HER2 protein expression in *Tsc1* cKO and *Tsc1* cre keratinocytes (**Figures 2E**, **S1D and S1E**). The intensity and duration of EGF-induced EGFR auto-phosphorylation was diminished in *Tsc1* cKO keratinocytes (**Figure 2F**), with dampened downstream signaling, as shown by decreased basal (**Figure 2E**; right panel) and EGF-stimulated ERK1/2 and AKT phosphorylation (**Figure 2F**). Despite these changes in total protein levels,

EGFR and HER2 mRNA levels were increased or unchanged in *Tsc1* cKO epidermis and keratinocytes (**figure S2A, B**), and in *Tsc1* cre keratinocytes (**figure S2C**) compared to their respective controls, suggesting post-transcriptional regulation.

Genetic and pharmacological inhibition of mTORC1 up-regulates EGFR and HER2 protein expression and activity

Studies in cancer cell lines and MEFs have demonstrated that mTORC1 inhibition results in increased PI3K/AKT/MAPK signaling via feedback activation of RTK signaling. This is mediated by mTORC1-dependent phosphorylation of RTK adaptor proteins (IRS-1, GRB10) (25-27) or altered expression of RTKs (IGFR/IR/PDGFR) (28, 29), however the mechanism of the latter effect on RTK expression is poorly understood. At least one prior study has shown that pharmacologic mTORC1 inhibition also leads to feedback activation of EGFR (30). We examined expression of EGFR and HER2 in mice with conditional epidermal loss of mTORC1 components *Rheb* or *Rptor,* as previously described (31). mTORC1 loss-of-function was confirmed by decreased p-p70 S6 Kinase and p-4E-BP1 levels in *Rptor* cre keratinocyte lysates by immunoblotting (**figure S2D**). Both *Rheb*$^{flox/flox}$/*Krt14-Cre (*<u>*Rheb* cKO</u>) keratinocytes as well as *Rptor* $^{flox/flox}$ keratinocytes infected with adenoviral cre recombinase (<u>*Rptor* cre</u>), up-regulated EGFR and HER2 protein expression compared to controls (**Figure 3A**). Membrane-localized EGFR and HER2 were concomitantly increased by immunofluorescence (**Figure 3B**) and surface biotinylation assays (**Figure 3C**). mTORC1 inhibitors (rapamycin, AZD8055 or Torin1) also elevated total (**Figure 3D**) and membrane (**Figure 3E**) EGFR and HER2 in WT keratinocytes. mTORC1 inactivation was associated with elevated EGF-stimulated EGFR auto-phosphorylation in *Rheb* cKO (**Figure 3F**), *Rptor* cre (**Figure 3G**) and AZD8055-treated (**Figure 3H**, **figure S9E**)

keratinocytes compared to controls, and with elevated and prolonged downstream ERK1/2 and AKT signaling in *Rheb* cKO and *Rptor* cre keratinocytes (**Figure 3F**, **figure S9A**, (31)). Finally, similar to *Tsc1* cKO keratinocytes, levels of EGFR and HER2 transcripts were minimally altered in *Rptor* cre keratinocytes (**figure S2E**), indicating a post-transcriptional mechanism of gene regulation. Thus, mTORC1 activity is both *necessary* and *sufficient* to regulate EGFR and HER2 total protein expression and activity in the epidermis.

mTORC1 stimulates EGF-induced EGFR degradation by promoting lysosomal biogenesis and activity

EGFR and HER2 levels are down-regulated by ligand-induced internalization and lysosomal-mediated degradation (32-34). We analyzed EGFR and HER2 degradation in response to exogenous EGF. Using high dose EGF to increase the rate of EGF-stimulated EGFR decay in control cells, EGFR degradation rate was significantly slowed in *Rptor* cre keratinocytes (**Figures 4A, B and S3A** using low dose EGF), *Rheb* cKO keratinocytes (**figure S3B and C**) and AZD8055-treated keratinocytes (**figure S3 D and E**). Conversely, using low dose EGF promoted only very minimal EGFR degradation in control keratinocytes, and the rate was significantly enhanced in *Tsc1* cKO keratinocytes (**Figure 4C, D**). These results raised the possibility that altered lysosomal degradation was mediating the EGFR levels with mTORC1 perturbation. Lysosomes are critical for the degradation of endocytosed or autophagocytosed cellular macromolecules. Lysosomal biogenesis is coordinated by the MiT/TFE subclass of basic helix-loop-helix transcription factors (TFEB/TFE3/MITF/TFEC), which drive transcription from consensus coordinated lysosomal expression and regulation (CLEAR) promoter elements on lysosomal/autophagy genes (5, 15, 35, 36). To investigate lysosomal gene-expression changes downstream of mTORC1 loss-of-function,

we performed microarray-based differential expression analysis of E18.5 epidermis from WT/ *Rptor* cKO mice. Out of 24,697 NCBI gene-annotated coding transcripts, we found 235 genes significantly (greater than 2 SD log2 fold change) upregulated and 941 downregulated in *Rptor* cKO compared with *Rptor* WT epidermis (**Supplemental Table 1**). We performed GSEA and found that a lysosomal gene signature panel (consisting of 360 lysosomal gene transcripts from the Mouse Lysosome Gene Database [mLGDB; http://lysosome.unipg.it/mouse.php]) was significantly negatively enriched in *Rptor* cKO epidermis (**Figure 4E**). We validated GSEA results by immunoblotting for multiple MiT/TFE-regulated lysosomal proteins, which were downregulated in *Rptor* cre and *Rheb* cKO keratinocytes compared to their respective controls (**Figures 4F**, **S4A and S4B**). Conversely, lysosomal/autophagy CLEAR target genes (36) were up-regulated in *Tsc1* cKO keratinocytes by qRT-PCR (**Figure 5A**) and in *Tsc1* cKO epidermis (**Figure 5B**) and keratinocyte (**Figure 5C**, **figure S4C**) immunoblots in an mTORC1-dependent manner (**Figure 5D**). CTSB/LAMP1 immunostaining revealed expansion of both lysosomal organelles in *Tsc1* cKO epidermis (**Figure 5E**). Treatment of *Tsc1* cre keratinocytes with the lysosomal V-ATPase inhibitor Bafilomycin A1 was sufficient to rescue EGFR expression, thus suggesting that increased lysosomal expression and/or activity was linked to EGFR loss in cells with constitutive mTORC1 signaling (**Figure 5F**).

We further characterized lysosomal protein localization by examining expression of lysosomal proteins in lysosomal-enriched fractions of keratinocyte lysates by immunoblotting, and found them to be increased in *Tsc1* cre keratinocytes and *Rheb1* S16H Tg keratinocytes relative to controls, and decreased in *Rptor* cre keratinocytes relative to controls (**Figure 6A).** Furthermore, the intensity of lysosomal LAMP2 (**Figure 6B)** and LAMP1 (**Figure 6C)** immunostaining was decreased in *Rptor* cre keratinocytes relative to controls. Quantification of fluorescent intensity

demonstrated a significant decrease in mean LAMP1 fluorescence in *Rptor* cre keratinocytes (**Figure 6D).** Finally, to assess the activity of lysosomal enzymes, we incubated cells with Magic Red CTSB, a cathepsin B substrate that produces a cresyl violet fluorophore upon proteolytic cleavage, and measured fluorescent intensity by fluorometry. CTSB activity was significantly decreased in *Rptor* cre keratinocytes, relative to controls (**Figure 6E).**

mTORC1 drives total MiT/TFE expression, nuclear localization and CLEAR promoter activity

To understand the basis for altered lysosomal gene expression/activity, we first queried total levels of MiT/TFE proteins which were increased in *Tsc1* cKO epidermis (**Figure 7A**) and keratinocytes in an mTORC1-sensitive manner (**Figure 7B**), and correspondingly decreased in *Rptor* cKO epidermis (**Figure 7C**), *Rptor* cre keratinocytes (**figure S5A**), and *Rheb* cKO keratinocytes (**figure S5B**). Furthermore, MiT/TFE proteins were highly enriched in nuclear fraction immunoblots of *Tsc1* cKO (**figure S5C**) and *Tsc1* cre (**Figure 7D, E**) keratinocytes in an mTORC1-dependent manner. TFE3 was also enriched in the basal nuclei of P7 *Tsc1* cKO epidermis by immunohistochemistry (**figure S5D**), and in the nuclei of *Tsc1* cre keratinocytes by immunofluorescence (**Figure 7F, G**) in an mTORC1-dependent manner (**figure S5E**). MiT/TFE proteins were correspondingly decreased in *Rptor* cre nuclei by nuclear lysate immunoblots (**figure S5F, G and H**) and immunofluorescence (**figure S5I**). Importantly, short-term Torin1 treatment (1hr) promoted, while long-term treatment (>24hr) decreased nuclear TFE3 by immunofluorescence (**figure S6A**). We then determined corresponding changes in CLEAR promoter element activity by transfecting cells with a 4X-CLEAR luciferase reporter construct (containing 4 tandem copies of a CLEAR promoter element) (37) and measuring luciferase activity. 4X-CLEAR transactivation was significantly higher in *Tsc1* cKO and *Tsc1* cre

keratinocytes **(Figure 7 H, I**) and lower in *Rptor* cre keratinocytes (**figure S6B**) compared to their respective controls, linking MiT/TFE levels, CLEAR promoter activity and altered lysosomal gene expression to mTORC1 status. Finally, in *Tsc1* cre keratinocytes, combined MiT/TFE (TFEB/TFE3/MITF) siRNA treatment or single siRNA against these genes repressed expression of many lysosomal CLEAR target genes and proteins, with TFE3 and TFEB appearing to drive most of the effects in triple knock-down treatment (**figures S6C, S7 and 7J**). Combined MiT/TFE knock-down was sufficient to rescue EGFR and HER2 expression (**Figure 7J**), thus linking increased MiT/TFE transcriptional activity to EGFR and HER2 loss in cells with constitutive mTORC1 signaling.

Inhibition of hyperactive AKT in mTORC1-inhibited cells rescues autophagy/ lysosomal biogenesis and downregulates EGFR expression

Taken together, these data indicate that prolonged increases in mTORC1 activity up-regulate lysosomal gene/protein expression via increased total and nuclear levels of MiTs and concomitant CLEAR promoter activity. Similarly, genetic or longer-term pharmacologic mTORC1 inhibition decreased MiT levels and activity and lysosomal gene transcription. Yet, these data are at odds with current models suggesting that mTORC1 suppression promotes MiT/TFE transcriptional activity (2-4). One mechanism for this apparent disconnect could be attributed to the activation of alternate signaling pathways bypassing mTORC1 or feedback loops downstream of mTORC1. For example *Tsc2*-deficient primary neurons showed increased autolysosome formation and autophagic flux via AMPK-dependent ULK1 activation, bypassing mTORC1-dependent ULK1 inhibition (38). Additionally, MiT/TFE activity can be co-regulated by numerous kinases including AKT (15-17). AKT phosphorylation at conserved RXXS/T motifs S467/S565/S510 in TFEB,

TFE3 and MITF respectively, results in their cytoplasmic retention/inactivation (17, 39) or proteasomal degradation (1, 40). We conducted a TMT-based phosphoproteomic analysis of control and *Rptor* KO keratinocytes, and found p-TFE3 (S564/565) levels to be significantly increased in *Rptor* KO keratinocytes compared to control (**figure S8**), raising the possibility that AKT was modulating TFE3 activity in the context of *Rptor* loss. Like mTORC1, AKT can negatively regulate autophagy and lysosomal biogenesis (17, 41). Thus, we tested whether AKT feedback activation in the context of long-term mTORC1 inhibition could inhibit MiT/TFE expression, nuclear localization and/or activity.

AKT activation was increased in *Rheb* cKO and *Rptor* cre keratinocytes (**Figure 3F**, **figure S9A**, (31)) and decreased in *Tsc1* cKO keratinocytes (**Figure 2E**, **F**), consistent with the presence of an mTORC1-AKT feedback loop as previously documented in other systems (26-28, 42, 43). Accordingly, incubation of *Rptor* cre keratinocytes with AKT kinase inhibitors MK2206 (**Figure 8A**) or GDC-0068 (**figure S9B**) rescued expression of lysosomal/ autophagy target genes, autophagic flux and MiT/TFE proteins in a dose-dependent manner. MK2206 treatment also the increased the number and perinuclear localization of lysosomes as seen by LAMP1 immunostaining and LysoTracker Red fluorescence (**Figure 8B, C**) and increased autophagic vesicles as seen by TEM (**Figure 8D**). This expansion of the lysosomal/autophagic compartment was driven by MiT/TFE activity since both MK2206 and GDC-0068 stimulated nuclear translocation of MiT/TFE proteins by immunoblot analyses (**Figure 8E, figure S9C**) and MK2206 also promoted 4X-CLEAR promoter transactivation in luciferase assays (**Figure 8F**). Correspondingly, MK2206, GDC-0068 and another AKT kinase inhibitor AZD5363, downregulated EGFR and HER2 protein expression in *Rptor* cre (**Figure 8G**, **figure S9D**) keratinocytes. PI3K inhibition using GDC-0941 in AZD8055-treated keratinocytes (**figure S9E**)

had a similar effect. Genetically silencing AKT1 or AKT2 in *Rptor* cre keratinocytes elevated lysosomal proteins and downregulated EGFR, validating the PI3K/AKT inhibitor results (**Figure 8H**). Conversely, adenoviral-mediated overexpression of constitutively activated myristolated (Myr)-AKT1 or AKT2 in *Tsc1* cKO keratinocytes downregulated lysosomal proteins and rescued EGFR and HER2 (**Figure 8I**). These findings confirmed that manipulation of AKT signaling, in the setting of mTORC1 loss or hyperactivity, was sufficient to alter MiT/TFE activity, lysosomal gene expression and cellular EGFR and HER2 levels.

Discussion

To study the effects of constitutive mTORC1 signaling activation or suppression in epithelial tissues, we developed genetically engineered mouse models that allow specific perturbation of mTORC1 signaling in epidermal keratinocytes. We found that mice with epidermal mTORC1 activation developed a phenotype strikingly similar to murine epidermal TGF-α or EGFR loss (20-22). Accordingly, *Tsc1* loss in the epidermis suppressed EGFR and HER2 expression and activity, while mTORC1 loss-of-function via pharmacological inactivation or *Rheb* or *Rptor* deletion in keratinocytes had the reverse effect. Among all surface receptors, EGFR signaling is prototypically regulated by ligand-induced lysosomal degradation. Significantly, the rate of EGFR decay was significantly enhanced in *Tsc1* cKO keratinocytes and decreased in mTORC1-inhibited keratinocytes, confirming that mTORC1 signaling was both necessary and sufficient to regulate the net rate of ligand-induced EGFR degradation.

Lysosomes are critical for the degradation of cellular macromolecules and are transcriptionally regulated by MiT/TFE family members. Interestingly, up-regulation of lysosomal function as well as mTORC1 activation are independently essential for epidermal differentiation and barrier function (18, 31). However, the interdependence of mTOR signaling and lysosomal function has not been studied in the skin. Unexpectedly, differential expression analyses comparing epidermis from WT and *Rptor* cKO mice revealed that lysosomal genes were significantly downregulated with mTORC1 loss-of-function in the epidermis. Accordingly, multiple lysosomal and autophagy CLEAR genes were upregulated with *Tsc1* loss and downregulated with mTORC1 loss-of-function. Probing further upstream, mTORC1 signaling was required to increase the expression, nuclear localization and transcriptional activity of MiTs, with a global increase in lysosomal content resulting in EGFR and HER2 downregulation.

Our findings that mTORC1 signaling was required to *activate* lysosomal biogenesis, were initially unexpected given the previously established role of mTORC1 as a short-term *negative* regulator of MiT/TFE-driven lysosomal biogenesis (2-6). We cannot exclude that our results may differ from previously published work in part because our studies used non-immortalized primary cells exclusively, while other studies were predominantly performed in murine embryonic fibroblasts. However, a number of different lines of evidence have since emerged to suggest that the role of mTORC1 in lysosomal gene regulation is likely much more complex than previously thought. First, though initial studies performed in a limited number of cell lines showed that MiT/TFE activity was increased following short-term mTORC1/2 inactivation with Torin1, short-term rapamycin did not affect TFEB phosphorylation or sub-cellular localization (3). While this could represent rapamycin-insensitive functions of mTORC1, the long-term effects of pharmacological mTORC1 inactivation have not been described thus far. We now show that Torin1 treatment in excess of 24 hours significantly decreases MiT/TFE transcriptional activity. In support of our findings, one previous study reported that temporal mTORC1 inactivation by Torin1 activated TFEB for a limited duration of 1.5 hours, following which it was progressively inactivated (44). Second, previous studies did not directly assess the impact of genetic or constitutive mTORC1 inactivation on lysosomal gene expression. We now show in an unbiased screen via GSEA, that mTORC1 loss-of-function in *Rptor* cKO epidermis down-regulates multiple lysosomal genes bearing CLEAR regulatory motifs. Finally, in the context of *Tsc*1/2 loss, several studies have suggested that constitutive activation of mTORC1 paradoxically positively regulates MiT/TFE localization and activity, though the mechanism was not elucidated. Pena-Llopis et al (11) showed that mTORC1 drives TFEB-dependent V-ATPase gene expression, further reinforcing their findings by publicly available gene expression data sets. Similarly, *Tsc*1/2 loss

promoted TFE3 nuclear localization in ESC cells, Eker rat kidneys and teratomas, in an mTORC1-dependent manner (12, 13).

How can we begin to reconcile these apparently conflicting data? Significantly, MiT/TFE localization is regulated by multiple mTORC1-independent signaling pathways, including ERK and AKT. ERK2-mediated phosphorylation of TFEB at S142 and AKT-mediated phosphorylation at S467/S565/S510 both promote cytosolic MiT/TFE retention and/or degradation (15, 17, 39, 40). Though these previous studies focused on the role of AKT in phosphorylation and nuclear translocation of MiT/TFE proteins, it is notable that we found both total and nuclear levels of MiT/TFEs to be proportionally affected by mTORC1 or AKT modulation. Thus, feedback activation of PI3K/AKT/MAPK signaling following long-term mTORC1 inhibition (25-27) could potentially restrain MiTs, competing with the direct effects of mTORC1. This could also explain why short-term Torin1 treatment promotes mTORC1-inhibited MiT/TFE nuclear localization (by also inhibiting AKT S473/T308 phosphorylation), while long-term treatment restrains mTORC1-inhibited MiT/TFE nuclear localization (via feedback up-regulation of AKT T308 phosphorylation) (43).

Consistent with this model, we observed the presence of an mTORC1-AKT negative feedback loop in epidermal keratinocytes. What factors could be driving feedback activation of AKT in the context of epidermal *Rheb* or *Rptor* loss? There are a number of known signaling intermediates (IRS-1, GRB10) and RTKs (HER3, IGFR, c-MET, PDGFR) which mediate this negative feedback signaling downstream of mTORC1 activity (25-29, 42, 43). Here, we show that EGFR signaling is itself activated downstream of AKT signaling via a decrease in MiT/TFE-mediated lysosomal biogenesis, further reinforcing this negative feedback to AKT. Accordingly, genetic and pharmacological inhibition of AKT in the context of *Rheb* or *Rptor* loss completely

rescued MiT/TFE-driven transcriptional activity, lysosomal biogenesis and down-regulated EGFR and HER2, while overexpression of constitutively activated AKT in *Tsc1* cKO keratinocytes downregulated lysosomal proteins and rescued EGFR and HER2. Notably, EGFR activation can independently trigger lysosomal dysfunction and mimic lysosomal storage diseases (45), potentially synergizing with hyperactive AKT in the context of mTORC1 loss-of-function.

Another unexpected finding in our study is that mTORC1 signaling perturbation modulated lysosomal biogenesis by effects on MiT/TFE levels. While most previous studies have suggested that MiT/TFE activity is regulated via phosphorylation-mediated changes in nuclear-cytoplasmic distribution, several lines of evidence support that altering total levels of these proteins is sufficient to modulate their activity. Gene rearrangements or gene amplifications involving *TFEB* or *MITF* result in massive over-expression and constitutive nuclear localization of the full-length TFEB/MITF protein in tumor cells and a similar mechanism occurs in *TFE3*-rearranged tumors (46). Though we focused on the study of primary, non-transformed epithelial cells, we observed that in addition to nuclear levels, *total* MiT/TFE protein levels were dramatically up-regulated with *Tsc1* loss in an mTORC1-sensitive manner and down-regulated with mTORC1 loss-of-function. AKT inhibition fully restored MiT/TFE transcriptional activity and concurrently elevated total levels of MiT/TFE proteins.

What are the potential mechanisms underlying mTORC1-mediated MiT/TFE protein expression and/or turnover? It is known that cellular protein degradation is performed by two major systems, the autophagy-lysosome system and the ubiquitin-proteasome system (UPS). These are interactive and compensatory, wherein impairment of one up-regulates the activity of the other (47). The UPS carries out degradation of both short-lived regulatory and misfolded proteins, and long-lived ones that form the bulk of the cell (48). However, the role of mTORC1 in

the regulation of UPS proteolysis is complex and contextual, since both mTORC1 inhibition (49, 50) and activation (51) can up-regulate proteasomal activity. One consequence of lysosomal/autophagy flux defects, seen in many lysosomal storage diseases, is the accumulation of poly-ubiquitinated proteins (52). Interestingly, AKT activation can increase the ubiquitination and proteasomal degradation of specific substrates (53, 54) via phosphorylation, and MiT/TFE proteins are known *bonafide* proteasomal substrates (55, 56) that can be targeted for degradation by phosphorylation via multiple kinases including AKT (40). Additionally, certain ubiquitin ligases involved in MiT/TFE regulation, such as STUB1 (56), are also responsible for the degradation of substrates in a PI3K/AKT-dependent manner (54). Further studies are required to determine the role of the UPS in MiT/TFE gene regulation, specific ubiquitin ligases or deubiquitinating enzymes (DUBs) modulating MiT/TFE turnover, the phospho-specific residues involved in this process and the role of PI3K/AKT signaling in mediating this effect.

In addition to enhancing our understanding of the role of mTORC1 signaling in the regulation of lysosomal biogenesis, our data have implications for keratinocyte differentiation and inflammatory skin disorders where mTOR signaling is frequently activated. There are several studies indicating that autophagy and lysosomal function are required for epidermal maturation (18, 57). Thus, the down-regulation of MiT/TFE expression and activity with mTORC1 loss-of-function may contribute to the keratinocyte differentiation and skin barrier defect we observed in previous work in the *Rptor* cKO mice (31). Accordingly, lysosomal dysfunction may also interfere with lipid biosynthesis, contributing to human skin disorders with defective barrier function such as atopic dermatitis (58). In other inflammatory disorders such as psoriasis, mTORC1 signaling is hyperactivated (59) and lysosomal function or dysfunction may contribute to aberrant epidermal homeostasis (60). In future studies, it will be of interest to investigate how changes in lysosomal

biology downstream of mTORC1 signaling may be mechanistically important and potential therapeutic targets in inflammatory skin disease.

Author contributions: Conceptualization and Design: AS, KA, TLL and PW. Data acquisition: KA, AS, SM, CHN, HK, ZK, MS, BL, CCT, BS and TLL. Data Analysis: KA, SM, CHN, AS, RA, CCT, BS, MS and TLL. Drafting of the manuscript: KA, SM, PP, CCT and TLL.

Acknowledgments: The authors thank Dr. Avi Rosenberg for assistance with analyzing TEM images and Dr. Paul Worley for providing us the *Rheb*$^{flox/flox}$ and *Rheb S16H* $^{flox/flox}$ mice.

Funding: This work was funded by the National Institutes of Health (R01 CA200858-01).

Declaration of Interests: The authors declare no competing interests or conflict of interest.

Methods:

Mice: Animal protocols were approved by the JHU Animal Care and Use Committee. The following strains were used:

1) Mice expressing cre recombinase under control of the human K14 promoter (*KRT14-cre*) (Stock Number 004782, STOCK Tg(*KRT14-cre*)1Amc/J) (The Jackson Laboratory).

2) Mice carrying loxP sites flanking exon 17 and 18 of *Tsc1*(Stock Number 005680, *Tsc1*^{tm1Djk}/J) (The Jackson Laboratory).

3) Mice carrying loxP sites flanking exon 2, 3 and 4 of *Tsc2*(Stock Number 027458, *Tsc2*$^{tm1.1Mjgk}$/J) (The Jackson Laboratory).

4) Mice with *lox*P-flanked *Rheb S16H* alleles were generated in the laboratory of P.F. Worley**.**

5) Mice carrying loxP sites flanking exon 6 of *Rptor* (Stock Number 013188, B6Cg-*Rptor*$^{tm1.1Dmsa}$/J) (The Jackson Laboratory).

6) Mice with *lox*P-flanked *Rheb1* alleles were generated in the laboratory of P.F. Worley**.**

Epidermal-specific deletion of *Tsc1* or transgenic expression of *Rheb S16H* was obtained by crossing homozygously-expressing *KRT14-cre* mice with *Tsc1* or *S16H fl/fl* mice. Epidermal-specific deletion of *Rheb* or *Rptor* was obtained by crossing hemizygously-expressing *KRT14-cre* mice with *Rheb* or *Rptor fl/fl* mice. All experiments were performed on E-18.5-E19.5 embryos and P0-P7 pups. Genomic DNA was isolated from tail snips and genotyping performed using the following primers:

-Wild-type and floxed *Tsc1*: 5'-GAA TCA ACC CCA CAG AGC AT-3' (forward)

5'-GTC ACG ACC GTA GGA GAA GC-3' (reverse)

-Floxed *S16H*: 5'-GCA ACG TGC TGG TTA TTG TG-3' (forward)

5’-GGG-GAA-CTT-CCT-GAC-TAG-GG-3’ (reverse)

-Excised *S16H*: 5’-CAG CCA TTG CCT TTT ATG GT-3’ (forward)

5’-ACC ACC ACC ACC ATT GAG AT-3’ (reverse)

-Wild-type and floxed *Rptor*: 5’-CTC AGT AGT GGT ATG TGC TCA G-3’ (forward)

5’-GGG TAC AGT ATG TCA GCA CAG-3’ (reverse)

-Wild-type and floxed *Rheb1:* 5’-GCC CAG AAC ATC TGT TCC AT-3’ (forward)

5’-GGT ACC CAC AAC CTG ACA CC-3’ (reverse)

-Recombined *Rheb1:* 5’-ATA GCT GGA GCC ACC AAC AC-3’ (forward)

5’-GCC TCA GCT TCT CAA GCA AC-3’ (reverse)

-KRT14-cre: 5’- TTC CTC AGG AGT GTC TTC GC-3’ (transgene)

5’-GTC CAT GTC CTT CCT GA GC-3’ (transgene)

5’-CAA ATG TTG CTT GTC TGG TG-3’ (internal positive control forward)

5’-GTC AGT CGA GTG CAC AGT TT-3’ (internal positive control reverse)

Primary mouse keratinocyte cultures: Primary mouse keratinocytes were isolated from newborn (P0/P7) skin. Newborn pups were decapitated, immersed in 7.5% povidone-iodine for 5 minutes and rinsed in 70% ethanol for 2 minutes. The trunk skin was removed and placed dermis-side down in a Petri dish containing 0.25% trypsin-EDTA (Invitrogen), overnight at 4 °C for 18h. The dermis was separated from the epidermis and keratinocytes isolated by scraping the basal surface of the epidermis. Keratinocyte cell suspensions were passed through a 100micron cell strainer, centrifugated twice and plated on Petri dishes coated with fibronectin (F1141; Sigma), in mouse keratinocyte medium (mKer) containing the following ingredients for a final volume of 500 ml:

1) 3 Parts Low glucose DMEM (337.5 ml)

2) 1 Part Ham's F-12 (112.5 ml)

3) 10% FBS (50 ml)

4) Penicillin (60 ug/ml) (1 ml of 10^4 units/ml stock)

5) Gentamycin (25 ug/ml) (250ul of 50 mg/ml stock)

6) Insulin (5 ug/ml) (250ul of 10 mg/ml stock)

7) Hydrocortisone (0.4 ug/ml) (200ul of 1 mg/ml stock)

8) Cholera Toxin (10^{-10} M) (5ul of 1 mg/ml stock)

9) Transferrin (5ug/ml) + 3,3-5'triiodo-L-thyronine (T3) ($2x10^{-9}$ M)
(500 ul of a T3-Transferrin stock)

To obtain keratinocytes with genetic ablation of *Rptor or Tsc1, Rptor*$^{flox/flox}$ or *Tsc1*$^{flox/flox}$ keratinocytes were infected with Cre-recombinase expressing or empty adenoviral vectors (Vector Biolabs), prior to plating cells.

Reagents and antibodies:

Primary antibodies:

Tsc1 (6935, Cell Signaling), 1:1000; **Tsc2** (3990, Cell Signaling), 1:1000; **Rheb** (09-247, Millipore), 1:1000; **Raptor** (2280, Cell Signaling), 1:1000; **Raptor** (05-1470, Millipore Sigma), 1:400; **Phospho-S6 Ribosomal Protein (Ser240/244)** (5364, Cell Signaling), 1:800-1:1000; **S6 Ribosomal Protein** (2317, Cell Signaling), 1:1000; **Phospho-4E BP1 (T37/46)** (2855, Cell Signaling), 1:1000; **4E-BP1** (9644, Cell Signaling), 1:1000; **Phospho-p70 S6 Kinase (T37/46)** (9205, Cell Signaling), 1:1000; **p70 S6 Kinase** (9202, Cell Signaling), 1:1000; **β-Actin** (3700, Cell Signaling), 1:4000; **Gapdh** (2118, Cell Signaling), 1:4000; **EGFR** (sc-03, Santa Cruz), 1:500; **HER2** (sc-284, Santa Cruz), 1:500; **p-EGFR(Y1068)** (2234, Cell Signaling), 1:250;

Phospho-Erk1/2 (9101, Cell Signaling), 1:1000; **Erk1/2** (4695, Cell Signaling), 1:1000; **Phospho-Akt (S473)** (4060, Cell Signaling), 1:1000; **Phospho-Akt (T308)** (5106, Cell Signaling), 1:500; **Akt (pan)** (4691, Cell Signaling), 1:1000; **Phospho-FoxO1 (Thr24)/FoxO3a (Thr32)/FoxO4 (Thr28)** (2599, Cell Signaling), 1:1000; **FoxO1** (2880, CellSignaling), 1:1000; **Na,K-ATPase** (3010, Cell Signaling), 1:1000; **LAMP-1** (sc-19992, Santa Cruz), 1:500; **LAMP-2** (ABL-93, DSHB at the University of Iowa), 1:50; **CTSB** (31718, Cell Signaling), 1:1000; **CTSD** (sc-6486, Santa Cruz), 1:500; **Rab7** (9367, Cell Signaling), 1:1000; **LAMTOR1** (8975, Cell Signaling), 1:1000; **LAMTOR2** (8145, Cell Signaling), 1:1000; **LAMTOR3** (8168, Cell Signaling), 1:1000; **RagA** (4357, Cell Signaling), 1:1000; **RagB** (8150, Cell Signaling), 1:1000; **RagC** (5466, Cell Signaling), 1:1000; **LAPTM4B** (ABC290, EMD Millipore), 1:1000; **p62/SQSTM1** (23214, Cell Signaling), 1:1000; **ATP6AP2** (10926-1-1AP, Proteintech), 1:500; **ATP6V0A1** (sc-374475, Santa Cruz), 1:500; **ATP6v1b1b2** (sc-374475, Santa Cruz), 1:500; **ATP6v1c1** (sc-271077, Santa Cruz), 1:500; **ATP6v1d** (sc-166218, Santa Cruz), 1:500; **Atg3** (3415, Cell Signaling), 1:1000; **Atg5** (12994, Cell Signaling), 1:1000; **Atg7** (8558, Cell Signaling), 1:1000; **Atg16L1** (8089, Cell Signaling), 1:1000; **TFEB** (A303-673A, Bethyl), 1:500; **TFE3** (PA5-54909, Thermo Fisher Scientific), 1:500**; TFE3** (ABE1400, Millipore Sigma), 1:500; **MITF** (10392-1-1AP, Proteintech), 1:500; **MITF** (12590, Cell Signaling), 1:500; **Histone H3** (4499, Cell Signaling), 1:1000; **Fibrillarin** (2639, Cell Signaling), 1:1000; **Lamin A/C** (4777, Cell Signaling), 1:1000; **Beclin-1** (3495, Cell Signaling), 1:1000; **LC3A** (4599, Cell Signaling), 1:1000.

Reagents: DMEM (11885084, Thermo Fisher Scientific), Ham's F-12 (11765054, Thermo Fisher Scientific), EGF (Peprotech), FBS (Hyclone), T3/Transferrin (Sigma), Hydrocortisone and Cholera toxin (Sigma), Insulin (Roche), Gentamycin (Amresco), Mg2+ lysis/wash buffer (20-

168, Millipore-Sigma), 8M Urea (Amresco), Cell lysis Buffer (9803, Cell Signaling), Rapamycin and AZD8055 (LC Laboratories), MK2206, GDC-0068, AZD8186 and GDC-0941 (Selleckchem) Torin1 and AKT1, 2 SignalSilence siRNA (Cell Signaling), Silencer Select Negative Control siRNA, Lipofectamine 3000 reagent, Lipofectamine RNAiMAX reagent LysoTracker DND-99 (Thermo Fisher Scientific), siGENOME Mouse siRNA SMARTpool (TFEB, TFE3 and MITF; Dharmacon), Adeno CMV Null, Cre Recombinase, Akt1 (Myr) and Akt2 (Myr) adenoviruses (Vector Biolabs), Magic Red Cathepsin B Kit (#ICT937, Biorad). 4XCLEAR-luciferase reporter was a gift from Albert La Spada (Addgene plasmid# 66880)(37).

Histology and immunostaining: Mouse skins were fixed in 10% neutral buffered formalin (Sigma-Aldrich), embedded in paraffin, sectioned at 4 μm and used for immunohistochemistry. Sections were deparaffinized in xylene (Sigma-Aldrich), hydrated in graded ethanol and rinsed in distilled water. Antigen retrieval was performed using citrate (10 mM, pH 6.0) or EDTA + 0.01% TWEEN 20 (1 mM, pH 8.0) buffers and HIER (heat-induced epitope retrieval) method, in accordance with the protocol specified for each antibody. All washing steps were done using 1X TBS-T buffer. Endogenous peroxidase activity was quenched by incubation with Dual Enzyme Block (Dako, Agilent Technologies) for 10 minutes at room temperature. Sections were incubated with each antibody overnight at 4°C diluted in antibody dilution buffer (Roche/ Ventana Medical Systems). For immunohistochemistry, a horseradish peroxidase–labeled polymer, Poly-HRP PowerVision Detection System (Novocastra/Leica Biosystems) was applied for 30 minutes at room temperature. Signal detection was performed using 3,3'-diaminobenzidine tetrahydrochloride (DAB) (Sigma-Aldrich) for 20 minutes at room temperature. Slides were counterstained for 30 seconds with Mayer's hematoxylin (Dako, Agilent Technologies), dehydrated, and mounted. For

592 immunofluorescence, after primary antibody overnight reaction at 4°C, sections were incubated
593 with secondary antibodies (Alexafluor-488 or Alexafluor-594 conjugated, anti-Rabbit or anti-
594 Mouse IgG, Thermo Fisher Scientific) at a dilution of 1:200 for 1h 30min at room temperature.
595 Subsequently they were washed 2x/5min in PBS, rinsed in distilled water, dehydrated in graded
596 ethanol and mounted with ProLong Gold Antifade with DAPI (Thermo Fisher Scientific). IHC for
597 TFE3 was carried out as previously described (61).
598

599 **Protein lysate preparation and immunoblotting:** Mouse epidermis was separated from the
600 dermis following incubation of pup skin with 3.8% Ammonium thiocynate (A7149, Sigma-
601 Aldrich) for 10 minutes at room temperature. The epidermal sheet was homogenized using
602 gentleMACS M tubes in the gentleMACS dissociator (Miltenyi Biotec). Tissues or cells were
603 homogenized and lysed in ice-cold 1X Mg2+ lysis/wash buffer (20-168, Millipore-Sigma) or
604 RIPA buffer (R0278, Sigma) supplemented with $NaVO_4$ (1 mM), NaF (1 mM) and 10 µl Halt
605 Protease and Phosphatase Inhibitor Cocktail (78440, Thermo Fisher Scientific) in 1 ml
606 buffer for 15 min on ice. Lysates were sheared by passing through 20, 22, 25 and 26 gauge needles
607 progressively, centrifuged at 21,000 rpm for 10 minutes at 4°C and supernatants collected. Protein
608 concentrations were quantified using the BCA Protein Assay Kit (23225, Pierce), and 5-10 ug of
609 protein was resolved on a 1.5-mm, 3-8% Tris-Acetate or 4-12% Bis-Tris SDS-PAGE gel (Thermo
610 Fisher Scientific). Protein was transferred to nitrocellulose membranes (Amersham Bioscience).
611 Membranes were allowed to block for 1h at room temperature in 5% nonfat milk in 1X TBS-T and
612 then incubated overnight with a primary antibody diluted in 5% BSA in 1X TBS-T. The secondary
613 antibodies used were anti-rabbit or anti-mouse immunoglobulin as appropriate (Cell Signaling)
614 and diluted at 1:1000 in 5% nonfat milk in 1X TBS-T. Blots were developed using a

chemiluminescent development solution (Super Signal West Femto, Pierce) and bands were imaged on a chemiluminescent imaging system (ChemiDoc Touch imaging System, Bio-Rad) or MicroChemi Chemiluminescent imager (FroggaBio Inc.). Digital images were quantified using background correction on the Alpha Innotech system (Protein Simple) and all bands were normalized to their respective β-actin, tubulin or GAPDH expression levels as loading controls. **Nuclear lysates** were prepared using the PARIS kit (AM1921, Thermo Fisher Scientific) according to manufacturer's instructions. Digital images were quantified using background correction on the Alpha Innotech system and all bands were normalized to their respective Lamin, Histone H3 or Fibrillarin levels as loading controls. **Cell surface biotinlyation** was performed using the Pierce Cell Surface Protein Isolation Kit (89881, Thermo Fisher Scientific) according to manufacturer's instructions. Digital images were quantified using background correction on the Alpha Innotech system and all bands were normalized to their respective Na/K-ATPase levels as loading controls. Statistical analysis was performed using Student's unpaired t-test.

siRNA-mediated gene silencing: Primary mouse keratinocytes were transfected with 50 nm siRNA using Lipofectamine RNAiMAX reagent using the reverse transfection protocol according to the transfection guidelines.

Plasmid transfection: Primary mouse keratinocytes were transfected Lipofectamine 3000 reagent (L3000008, Thermo Fisher Scientific) according to the transfection guidelines.

RNA isolation and quantitative real-time RT-PCR: Total cellular RNA was extracted using either TRIzol (15596026, Invitrogen) for epidermal tissue, or RNeasy Mini kit (74104, Qiagen)

for keratinocytes according to manufacturer's instructions. RNA was converted to cDNA using SuperScript III First-Strand Synthesis System (18080051, Thermo Fisher Scientific) according to manufacturer's instructions. mRNA levels were quantified using an ABI Prism 7900HT Real-time PCR system (Applied Biosystems) with the following primers and probes: **ATP6AP2**(Mm00510396_m1), **ATP6V0A** (Mm00441838_m1), **ATP6V0B** (Mm00504328_m1), **ATP6V1A** (Mm01343719_m1), **ATP6V1B2** (Mm00431987_m1), **ATP6V1C2** (Mm00505047_m1), **ATP6V1D** (Mm00445832_m1), **ATP6V1E1** (Mm00657610_m1), **LAMP1** (Mm00495262_m1), **CTSB** (Mm01310506_m1), **CTSD** (Mm00515586_m1), **CTSK** (Mm00484039_m1), **MCOLN1** (Mm00522550_m1), **SQSTM1** (Mm00448091_m1), **TFEB** (Mm00448968_m1), **TFE3** (Mm01341186_m1), **MITF** (Mm00434954_m1), **EGFR** (Mm01187858_m1), **ERBB2** (Mm00658541_m1), **ACTB** (Mm02619850_m1). Threshold cycle (Ct) was obtained from the PCR reaction curves and mRNA levels were quantitated using the comparative Ct method with actin mRNA serving as the reference. Statistical analysis was performed using Student's unpaired t-test.

Lysosomal expression and activity assays: Lysosomal fractionation assays-were carried out as previously described (62). Cultured keratinocytes grown on 150 mm dishes were harvested and lysed in 750 ml of cold fractionation buffer (50 mM KCl, 90 mM potassium gluconate, 1 mM EGTA, 50 mM sucrose, 5 mM glucose, protease inhibitor cocktail tablet and 20 mM HEPES, pH 7.4). The cells were then lysed by syringing, and nuclear fraction was removed by centrifugation at 1,000 g for 10 min at 4 C. The supernatant was then centrifuged at 20,000 g for 30 min at 4 C. The precipitated lysosome-enriched fraction (LEF) was resuspended in the fractionation buffer, and the supernatant was separated as the cytosolic fraction. **Cathepsin B activity assays-** To

662 measure lysosomal Cathepsin B activity, cells were incubated with Magic Red Cathepsin B
663 (Biorad), for 1 hr and processed according to the manufacturer's instructions for fluorescence plate
664 reader analysis.
665
666 **Immunocytochemistry:** Primary mouse keratinocytes were seeded on coverslips coated with
667 fibronectin. Following experimental treatments, cells were either fixed in 100% methanol at -20°C
668 for 30 minutes or 4% PFA for 15 minutes at room temperature, according to antibody
669 specifications. Following three rinses in 1X PBS, cells were permeabilized and blocked in a buffer
670 containing 1X PBS, 5% normal donkey serum and 0.3% Triton X-100. For immunofluorescence,
671 coverslips were incubated with the indicated primary antibodies overnight at 4°C in antibody
672 dilution buffer (ADB) containing 1X PBS, 1% BSA and 0.3% Triton X-100. After 3 rinses of 1X
673 PBS, coverslips were incubated with secondary antibodies (Alexafluor-488 or Alexafluor-594
674 conjugated, anti-Rabbit or anti-Mouse IgG, Thermo Fisher Scientific) in ADB at a dilution of
675 1:200 for 1 hour at room temperature. Nuclei were counterstained with DAPI and coverslips
676 visualized using an Olympus BX41 epifluorescence microscope (Olympus, Center Valley, PA).
677
678 **Immunofluorescence image analysis and quantifications:** Image analysis and quantification
679 was done in ImageJ. **Lamp1 immunostaining and quantification**: Confocal images were
680 acquired on a Nikon TE-2000e microscope and using the NIS elements 5.0.1 software. All images
681 were captured using the same exposure and gain settings followed by automatic de-
682 convolution. The area of Lamp1 was measured using Image J and normalized to the number of
683 nuclei. **Quantification of nuclear TFE3 intensity:** Cells were stained with DAPI to mark nuclei
684 (blue channel) and anti-total TFE3 (red channel). Images were analyzed using ImageJ. The blue

channel was used to segment nuclei as follows: images were thresholded to remove background and converted to binary images, following which the analyze Particles function was used for automatic detection of nuclear outlines. These nuclear outlines were applied to the red channel and mean fluorescence intensity of TFE3 within the regions was measured. **Statistics for image analysis:** Normal distribution was assessed using the D'Agostino & Pearson normality test. If normally distributed, statistical significance was determined with Student's t-test when comparing two experimental groups, or with one-way ANOVA with Dunnett's correction when comparing 3 or more experimental groups. If not normally distributed, statistical significance was determined with the Mann-Whitney test when comparing two experimental groups, or with the Kurskal-Wallis test with Dunn's correction when comparing 3 or more experimental groups. All tests assumed a two-tailed deviation and were performed in Prism 7 (GraphPad).

Transmission Electron Microscopy: Mouse skin and keratinocyte samples were fixed in 2.5% glutaraldehyde, 3mM $MgCl_2$ and 1% sucrose, in 0.1 M sodium cacodylate buffer, pH 7.2 at 4ºC overnight, followed by 3 buffer rinses, 15 minutes each, in 3mM $MgCl_2$, 3% sucrose and 0.1 M sodium cacodylate. The samples were post-fixed in 1% osmium tetroxide in 0.1 M sodium cacodylate for 1 hour on ice in the dark, rinsed twice with distilled water for 5 minutes, stained with 2% aqueous uranyl acetate (0.22 µm filtered) for 1 hour in the dark, followed by dehydration in an ascending grade of ethanol (50%, 70%, 90% and 100%; thrice each) and embedded in an epoxy resin. The resin was allowed to polymerize at 37ºC overnight for 2-3 days followed by 60ºC overnight. Grids were stained with 2% uranyl acetate in 50% methanol, followed by lead citrate, and observed with a Philips CM120 at 80kV. Images were captured with an AMT XR80 high-resolution (16-bit) 8 Mpixel camera.

Microarray analysis: Microarray-based differential expression analysis of E18.5 epidermis from WT/ *Rptor* cKO mice was carried out as described in Supplemental methods. (GEO accession number 124754)

Statistics: For image analysis, RNA and protein quantification and luciferase assays, statistical significance was determined using the unpaired, two-tailed Student's t-test when comparing two experimental groups, or with one-way ANOVA with Tukey's correction when comparing 3 or more experimental groups. All tests were performed in Prism 8 (GraphPad). p-values of <0.05 were considered statistically significant.

Phosphoproteome analysis: TMT-based phosphoprotoeme analysis of control or *Rptor* KO mouse primary keratinocytes was carried out as described in Supplemental methods.

References:

1. Puertollano R, Ferguson SM, Brugarolas J, and Ballabio A. The complex relationship between TFEB transcription factor phosphorylation and subcellular localization. *Embo j.* 2018;37(11).
2. Roczniak-Ferguson A, Petit CS, Froehlich F, Qian S, Ky J, Angarola B, Walther TC, and Ferguson SM. The transcription factor TFEB links mTORC1 signaling to transcriptional control of lysosome homeostasis. *Sci Signal.* 2012;5(228):ra42.
3. Settembre C, Zoncu R, Medina DL, Vetrini F, Erdin S, Erdin S, Huynh T, Ferron M, Karsenty G, Vellard MC, et al. A lysosome-to-nucleus signalling mechanism senses and regulates the lysosome via mTOR and TFEB. *EMBO J.* 2012;31(5):1095-108.
4. Martina JA, Chen Y, Gucek M, and Puertollano R. MTORC1 functions as a transcriptional regulator of autophagy by preventing nuclear transport of TFEB. *Autophagy.* 2012;8(6):903-14.
5. Martina JA, Diab HI, Lishu L, Jeong AL, Patange S, Raben N, and Puertollano R. The nutrient-responsive transcription factor TFE3 promotes autophagy, lysosomal biogenesis, and clearance of cellular debris. *Sci Signal.* 2014;7(309):ra9.
6. Napolitano G, Esposito A, Choi H, Matarese M, Benedetti V, Di Malta C, Monfregola J, Medina DL, Lippincott-Schwartz J, and Ballabio A. mTOR-dependent phosphorylation controls TFEB nuclear export. *Nat Commun.* 2018;9(1):3312.
7. Saxton RA, and Sabatini DM. mTOR Signaling in Growth, Metabolism, and Disease. *Cell.* 2017;168(6):960-76.
8. Yu L, McPhee CK, Zheng L, Mardones GA, Rong Y, Peng J, Mi N, Zhao Y, Liu Z, Wan F, et al. Termination of autophagy and reformation of lysosomes regulated by mTOR. *Nature.* 2010;465(7300):942-6.
9. Baar K, and Esser K. Phosphorylation of p70(S6k) correlates with increased skeletal muscle mass following resistance exercise. *The American journal of physiology.* 1999;276(1 Pt 1):C120-7.
10. Mansueto G, Armani A, Viscomi C, D'Orsi L, De Cegli R, Polishchuk EV, Lamperti C, Di Meo I, Romanello V, Marchet S, et al. Transcription Factor EB Controls Metabolic Flexibility during Exercise. *Cell Metab.* 2017;25(1):182-96.
11. Pena-Llopis S, Vega-Rubin-de-Celis S, Schwartz JC, Wolff NC, Tran TA, Zou L, Xie XJ, Corey DR, and Brugarolas J. Regulation of TFEB and V-ATPases by mTORC1. *EMBO J.* 2011;30(16):3242-58.
12. Betschinger J, Nichols J, Dietmann S, Corrin PD, Paddison PJ, and Smith A. Exit from pluripotency is gated by intracellular redistribution of the bHLH transcription factor Tfe3. *Cell.* 2013;153(2):335-47.
13. Kawano H, Ito Y, Kanai F, Nakamura E, Tada N, Takai S, Horie S, Kobayashi T, and Hino O. Aberrant differentiation of Tsc2-deficient teratomas associated with activation of the mTORC1-TFE3 pathway. *Oncology reports.* 2015;34(5):2251-8.
14. Di Malta C, Siciliano D, Calcagni A, Monfregola J, Punzi S, Pastore N, Eastes AN, Davis O, De Cegli R, Zampelli A, et al. Transcriptional activation of RagD GTPase controls mTORC1 and promotes cancer growth. *Science.* 2017;356(6343):1188-92.
15. Settembre C, Di Malta C, Polito VA, Garcia Arencibia M, Vetrini F, Erdin S, Erdin SU, Huynh T, Medina D, Colella P, et al. TFEB links autophagy to lysosomal biogenesis. *Science.* 2011;332(6036):1429-33.
16. Li Y, Xu M, Ding X, Yan C, Song Z, Chen L, Huang X, Wang X, Jian Y, Tang G, et al. Protein kinase C controls lysosome biogenesis independently of mTORC1. *Nat Cell Biol.* 2016;18(10):1065-77.
17. Palmieri M, Pal R, Nelvagal HR, Lotfi P, Stinnett GR, Seymour ML, Chaudhury A, Bajaj L, Bondar VV, Bremner L, et al. mTORC1-independent TFEB activation via Akt inhibition promotes cellular clearance in neurodegenerative storage diseases. *Nat Commun.* 2017;8(14338.
18. Monteleon CL, Agnihotri T, Dahal A, Liu M, Rebecca VW, Beatty GL, Amaravadi RK, and Ridky TW. Lysosomes Support the Degradation, Signaling, and Mitochondrial Metabolism Necessary for Human Epidermal Differentiation. *J Invest Dermatol.* 2018;138(9):1945-54.
19. Kobayashi T, Minowa O, Sugitani Y, Takai S, Mitani H, Kobayashi E, Noda T, and Hino O. A germ-line Tsc1 mutation causes tumor development and embryonic lethality that are similar, but not identical to, those caused by Tsc2 mutation in mice. *Proc Natl Acad Sci U S A.* 2001;98(15):8762-7.
20. Luetteke NC, Qiu TH, Peiffer RL, Oliver P, Smithies O, and Lee DC. TGF alpha deficiency results in hair follicle and eye abnormalities in targeted and waved-1 mice. *Cell.* 1993;73(2):263-78.
21. Lichtenberger BM, Gerber PA, Holcmann M, Buhren BA, Amberg N, Smolle V, Schrumpf H, Boelke E, Ansari P, Mackenzie C, et al. Epidermal EGFR controls cutaneous host defense and prevents inflammation. *Sci Transl Med.* 2013;5(199):199ra11.

22. Schneider MR, Werner S, Paus R, and Wolf E. Beyond wavy hairs: the epidermal growth factor receptor and its ligands in skin biology and pathology. *Am J Pathol.* 2008;173(1):14-24.
23. Zou J, Zhou L, Du XX, Ji Y, Xu J, Tian J, Jiang W, Zou Y, Yu S, Gan L, et al. Rheb1 is required for mTORC1 and myelination in postnatal brain development. *Dev Cell.* 2011;20(1):97-108.
24. Chong-Kopera H, Inoki K, Li Y, Zhu T, Garcia-Gonzalo FR, Rosa JL, and Guan KL. TSC1 stabilizes TSC2 by inhibiting the interaction between TSC2 and the HERC1 ubiquitin ligase. *J Biol Chem.* 2006;281(13):8313-6.
25. Carracedo A, Ma L, Teruya-Feldstein J, Rojo F, Salmena L, Alimonti A, Egia A, Sasaki AT, Thomas G, Kozma SC, et al. Inhibition of mTORC1 leads to MAPK pathway activation through a PI3K-dependent feedback loop in human cancer. *J Clin Invest.* 2008;118(9):3065-74.
26. Harrington LS, Findlay GM, Gray A, Tolkacheva T, Wigfield S, Rebholz H, Barnett J, Leslie NR, Cheng S, Shepherd PR, et al. The TSC1-2 tumor suppressor controls insulin-PI3K signaling via regulation of IRS proteins. *J Cell Biol.* 2004;166(2):213-23.
27. Yu Y, Yoon SO, Poulogiannis G, Yang Q, Ma XM, Villen J, Kubica N, Hoffman GR, Cantley LC, Gygi SP, et al. Phosphoproteomic analysis identifies Grb10 as an mTORC1 substrate that negatively regulates insulin signaling. *Science.* 2011;332(6035):1322-6.
28. Zhang H, Bajraszewski N, Wu E, Wang H, Moseman AP, Dabora SL, Griffin JD, and Kwiatkowski DJ. PDGFRs are critical for PI3K/Akt activation and negatively regulated by mTOR. *J Clin Invest.* 2007;117(3):730-8.
29. Muranen T, Selfors LM, Worster DT, Iwanicki MP, Song L, Morales FC, Gao S, Mills GB, and Brugge JS. Inhibition of PI3K/mTOR leads to adaptive resistance in matrix-attached cancer cells. *Cancer Cell.* 2012;21(2):227-39.
30. Wei F, Zhang Y, Geng L, Zhang P, Wang G, and Liu Y. mTOR inhibition induces EGFR feedback activation in association with its resistance to human pancreatic cancer. *International journal of molecular sciences.* 2015;16(2):3267-82.
31. Asrani K, Sood A, Torres A, Georgess D, Phatak P, Kaur H, Dubin A, Talbot CC, Jr., Elhelu L, Ewald AJ, et al. mTORC1 loss impairs epidermal adhesion via TGF-beta/Rho kinase activation. *J Clin Invest.* 2017;127(11):4001-17.
32. Goh LK, and Sorkin A. Endocytosis of receptor tyrosine kinases. *Cold Spring Harb Perspect Biol.* 2013;5(5):a017459.
33. Longva KE, Blystad FD, Stang E, Larsen AM, Johannessen LE, and Madshus IH. Ubiquitination and proteasomal activity is required for transport of the EGF receptor to inner membranes of multivesicular bodies. *J Cell Biol.* 2002;156(5):843-54.
34. Sigismund S, Algisi V, Nappo G, Conte A, Pascolutti R, Cuomo A, Bonaldi T, Argenzio E, Verhoef LG, Maspero E, et al. Threshold-controlled ubiquitination of the EGFR directs receptor fate. *Embo j.* 2013;32(15):2140-57.
35. Perera RM, Stoykova S, Nicolay BN, Ross KN, Fitamant J, Boukhali M, Lengrand J, Deshpande V, Selig MK, Ferrone CR, et al. Transcriptional control of autophagy-lysosome function drives pancreatic cancer metabolism. *Nature.* 2015;524(7565):361-5.
36. Palmieri M, Impey S, Kang H, di Ronza A, Pelz C, Sardiello M, and Ballabio A. Characterization of the CLEAR network reveals an integrated control of cellular clearance pathways. *Hum Mol Genet.* 2011;20(19):3852-66.
37. Cortes CJ, Miranda HC, Frankowski H, Batlevi Y, Young JE, Le A, Ivanov N, Sopher BL, Carromeu C, Muotri AR, et al. Polyglutamine-expanded androgen receptor interferes with TFEB to elicit autophagy defects in SBMA. *Nat Neurosci.* 2014;17(9):1180-9.
38. Di Nardo A, Wertz MH, Kwiatkowski E, Tsai PT, Leech JD, Greene-Colozzi E, Goto J, Dilsiz P, Talos DM, Clish CB, et al. Neuronal Tsc1/2 complex controls autophagy through AMPK-dependent regulation of ULK1. *Hum Mol Genet.* 2014;23(14):3865-74.
39. Pi H, Li M, Zou L, Yang M, Deng P, Fan T, Liu M, Tian L, Tu M, Xie J, et al. AKT inhibition-mediated dephosphorylation of TFE3 promotes overactive autophagy independent of MTORC1 in cadmium-exposed bone mesenchymal stem cells. *Autophagy.* 2018:1-18.
40. Wang C, Zhao L, Su Q, Fan X, Wang Y, Gao S, Wang H, Chen H, Chan CB, and Liu Z. Phosphorylation of MITF by AKT affects its downstream targets and causes TP53-dependent cell senescence. *The international journal of biochemistry & cell biology.* 2016;80(132-42.

41. Wang RC, Wei Y, An Z, Zou Z, Xiao G, Bhagat G, White M, Reichelt J, and Levine B. Akt-mediated regulation of autophagy and tumorigenesis through Beclin 1 phosphorylation. *Science.* 2012;338(6109):956-9.
42. Rodrik-Outmezguine VS, Chandarlapaty S, Pagano NC, Poulikakos PI, Scaltriti M, Moskatel E, Baselga J, Guichard S, and Rosen N. mTOR kinase inhibition causes feedback-dependent biphasic regulation of AKT signaling. *Cancer Discov.* 2011;1(3):248-59.
43. Yoon SO, Shin S, Karreth FA, Buel GR, Jedrychowski MP, Plas DR, Dedhar S, Gygi SP, Roux PP, Dephoure N, et al. Focal Adhesion- and IGF1R-Dependent Survival and Migratory Pathways Mediate Tumor Resistance to mTORC1/2 Inhibition. *Mol Cell.* 2017;67(3):512-27.e4.
44. Marin Zapata PA, Beese CJ, Junger A, Dalmasso G, Brady NR, and Hamacher-Brady A. Time course decomposition of cell heterogeneity in TFEB signaling states reveals homeostatic mechanisms restricting the magnitude and duration of TFEB responses to mTOR activity modulation. *BMC cancer.* 2016;16(355.
45. De Pasquale V, Pezone A, Sarogni P, Tramontano A, Schiattarella GG, Avvedimento VE, Paladino S, and Pavone LM. EGFR activation triggers cellular hypertrophy and lysosomal disease in NAGLU-depleted cardiomyoblasts, mimicking the hallmarks of mucopolysaccharidosis IIIB. *Cell death & disease.* 2018;9(2):40.
46. Kauffman EC, Ricketts CJ, Rais-Bahrami S, Yang Y, Merino MJ, Bottaro DP, Srinivasan R, and Linehan WM. Molecular genetics and cellular features of TFE3 and TFEB fusion kidney cancers. *Nature reviews Urology.* 2014;11(8):465-75.
47. Pandey UB, Nie Z, Batlevi Y, McCray BA, Ritson GP, Nedelsky NB, Schwartz SL, DiProspero NA, Knight MA, Schuldiner O, et al. HDAC6 rescues neurodegeneration and provides an essential link between autophagy and the UPS. *Nature.* 2007;447(7146):859-63.
48. Rock KL, Gramm C, Rothstein L, Clark K, Stein R, Dick L, Hwang D, and Goldberg AL. Inhibitors of the proteasome block the degradation of most cell proteins and the generation of peptides presented on MHC class I molecules. *Cell.* 1994;78(5):761-71.
49. Zhao J, Zhai B, Gygi SP, and Goldberg AL. mTOR inhibition activates overall protein degradation by the ubiquitin proteasome system as well as by autophagy. *Proc Natl Acad Sci U S A.* 2015;112(52):15790-7.
50. Rousseau A, and Bertolotti A. An evolutionarily conserved pathway controls proteasome homeostasis. *Nature.* 2016;536(7615):184-9.
51. Zhang Y, Nicholatos J, Dreier JR, Ricoult SJ, Widenmaier SB, Hotamisligil GS, Kwiatkowski DJ, and Manning BD. Coordinated regulation of protein synthesis and degradation by mTORC1. *Nature.* 2014;513(7518):440-3.
52. Komatsu M, Waguri S, Chiba T, Murata S, Iwata J, Tanida I, Ueno T, Koike M, Uchiyama Y, Kominami E, et al. Loss of autophagy in the central nervous system causes neurodegeneration in mice. *Nature.* 2006;441(7095):880-4.
53. Aoki M, Jiang H, and Vogt PK. Proteasomal degradation of the FoxO1 transcriptional regulator in cells transformed by the P3k and Akt oncoproteins. *Proc Natl Acad Sci U S A.* 2004;101(37):13613-7.
54. Terme JM, Lhermitte L, Asnafi V, and Jalinot P. TGF-beta induces degradation of TAL1/SCL by the ubiquitin-proteasome pathway through AKT-mediated phosphorylation. *Blood.* 2009;113(26):6695-8.
55. Zhao X, Fiske B, Kawakami A, Li J, and Fisher DE. Regulation of MITF stability by the USP13 deubiquitinase. *Nat Commun.* 2011;2(414.
56. Sha Y, Rao L, Settembre C, Ballabio A, and Eissa NT. STUB1 regulates TFEB-induced autophagy-lysosome pathway. *EMBO J.* 2017;36(17):2544-52.
57. Yoshihara N, Ueno T, Takagi A, Oliva Trejo JA, Haruna K, Suga Y, Komatsu M, Tanaka K, and Ikeda S. The significant role of autophagy in the granular layer in normal skin differentiation and hair growth. *Arch Dermatol Res.* 2015;307(2):159-69.
58. Elias PM, and Wakefield JS. Mechanisms of abnormal lamellar body secretion and the dysfunctional skin barrier in patients with atopic dermatitis. *J Allergy Clin Immunol.* 2014;134(4):781-91 e1.
59. Buerger C, Shirsath N, Lang V, Berard A, Diehl S, Kaufmann R, Boehncke WH, and Wolf P. Inflammation dependent mTORC1 signaling interferes with the switch from keratinocyte proliferation to differentiation. *PLoS One.* 2017;12(7):e0180853.
60. Akinduro O, Sully K, Patel A, Robinson DJ, Chikh A, McPhail G, Braun KM, Philpott MP, Harwood CA, Byrne C, et al. Constitutive Autophagy and Nucleophagy during Epidermal Differentiation. *J Invest Dermatol.* 2016;136(7):1460-70.

61. Argani P, Aulmann S, Illei PB, Netto GJ, Ro J, Cho HY, Dogan S, Ladanyi M, Martignoni G, Goldblum JR, et al. A distinctive subset of PEComas harbors TFE3 gene fusions. *Am J Surg Pathol.* 2010;34(10):1395-406.
62. Kim YC, Park HW, Sciarretta S, Mo JS, Jewell JL, Russell RC, Wu X, Sadoshima J, and Guan KL. Rag GTPases are cardioprotective by regulating lysosomal function. *Nat Commun.* 2014;5(4241.

Figure 1

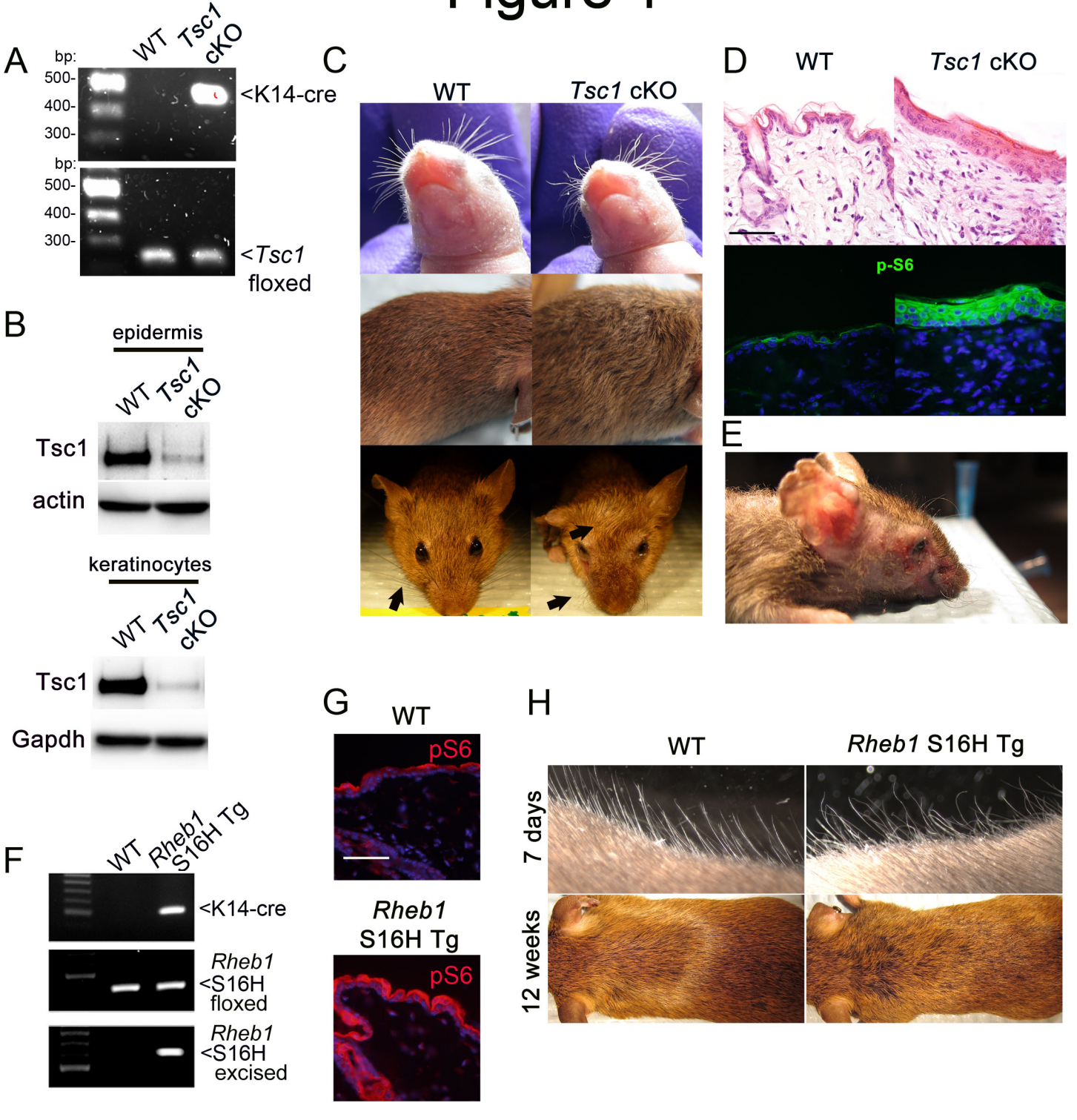
A
WT
Tsc1 cKO
bp:
500-
400-
300-
<K14-cre
bp:
500-
400-
300-
<Tsc1 floxed
B
epidermis
WT
Tsc1 cKO
Tsc1
actin
keratinocytes
WT
Tsc1 cKO
Tsc1
Gapdh
C
WT
Tsc1 cKO
D
WT
Tsc1 cKO
p-S6
E
F
WT
Rheb1 S16H Tg
<K14-cre
Rheb1 <S16H floxed
Rheb1 <S16H excised
G
WT
pS6
Rheb1 S16H Tg
pS6
H
WT
Rheb1 S16H Tg
7 days
12 weeks

Main Figure Legends

Figure 1: Epidermal-specific mTORC1 gain-of-function models have skin defects reminiscent of epidermal EGFR or TGFα loss. (A) Genotyping PCR of genomic tail DNA from WT and *Tsc1* cKO mice showing presence of *Tsc1* $^{flox/flox}$ alleles and *Krt14-Cre in Tsc1* cKO mice. **(B)** Immunoblotting of WT and *Tsc1* cKO epidermal and keratinocyte lysates for Tsc1. **(C)** *Tsc1* cKO pups show curly whiskers at birth (top panel) and wavy fur at 4 weeks (middle, bottom panels). **(D)** *Tsc1* cKO mice show thickened epidermis on histology (top panel) and increased mTORC1 activity as seen by p-S6 immunofluorescence (bottom panel). Scale bar=150 μm. **(E)** *Tsc1* cKO mice develop severe dermatitis in the facial region by 6 months. **(F)** Genotyping PCR of genomic tail DNA from WT and *Rheb1* S16H Tg mice showing presence of *Rheb1* S16H $^{flox/flox}$ alleles, *Rheb1* S16H excision alleles and Krt14-Cre in *Rheb1* S16H Tg mice. *Rheb1 S16H* transgenic mice show increased mTORC1 activity as seen by **(G)** p-S6 immunofluorescence. Scale bar=150 μm **(H)** *Rheb1 S16H* transgenic mice show presence of wavy fur, similar to *Tsc1* cKO mice.

Figure 2

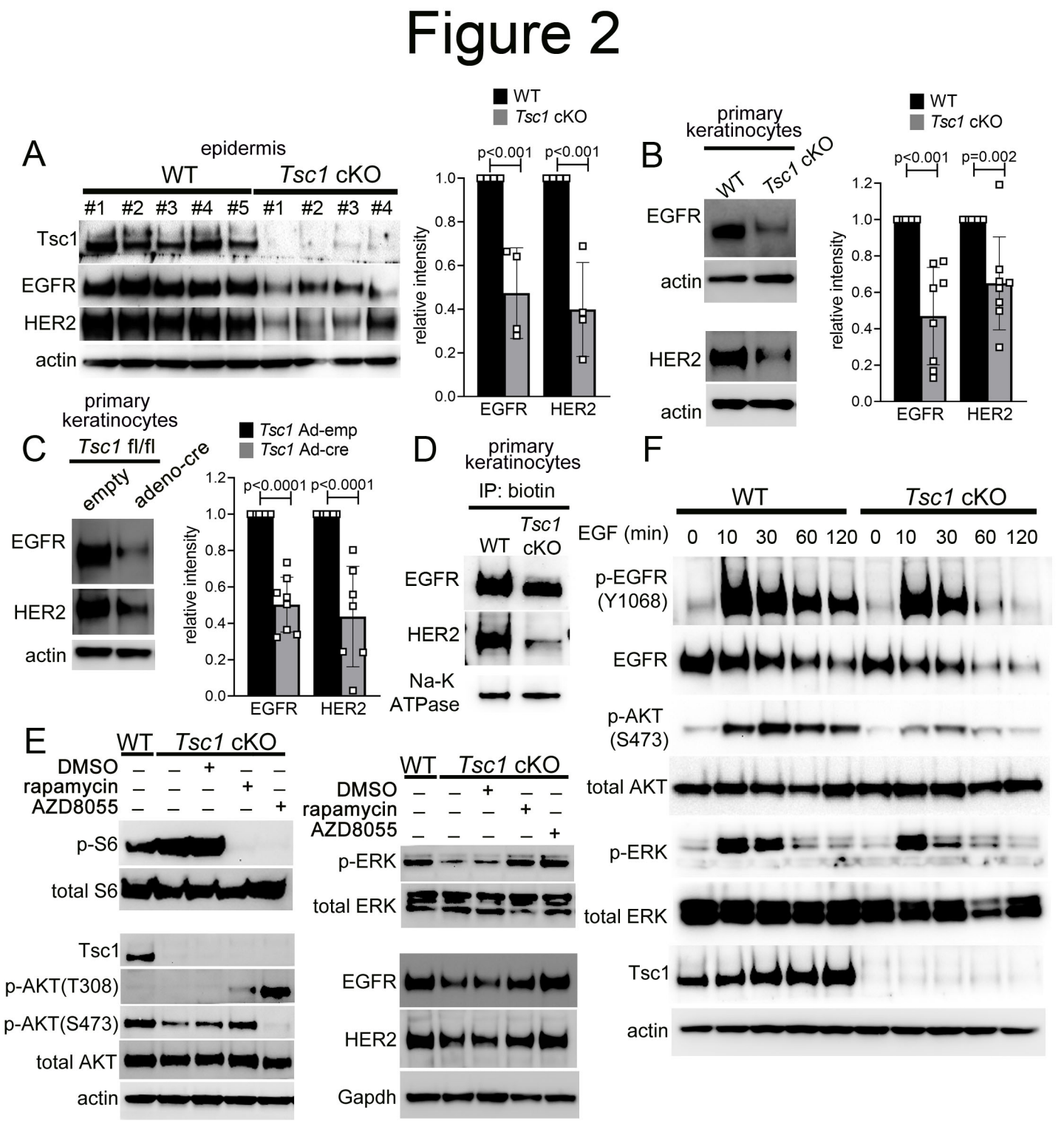
A
epidermis
WT
Tsc1 cKO
#1 #2 #3 #4 #5 #1 #2 #3 #4
Tsc1
EGFR
HER2
actin
WT
Tsc1 cKO
p<0.001 p<0.001
relative intensity
EGFR HER2
B
primary keratinocytes
WT
Tsc1 cKO
EGFR
actin
HER2
actin
WT
Tsc1 cKO
p<0.001 p=0.002
relative intensity
EGFR HER2
C
primary keratinocytes
Tsc1 fl/fl
empty
adeno-cre
EGFR
HER2
actin
Tsc1 Ad-emp
Tsc1 Ad-cre
p<0.0001 p<0.0001
relative intensity
EGFR HER2
D
primary keratinocytes
IP: biotin
WT
Tsc1 cKO
EGFR
HER2
Na-K ATPase
F
WT
Tsc1 cKO
EGF (min)
0 10 30 60 120 0 10 30 60 120
p-EGFR (Y1068)
EGFR
p-AKT (S473)
total AKT
p-ERK
total ERK
Tsc1
actin
E
WT
Tsc1 cKO
DMSO
rapamycin
AZD8055
p-S6
total S6
Tsc1
p-AKT(T308)
p-AKT(S473)
total AKT
actin
WT
Tsc1 cKO
DMSO
rapamycin
AZD8055
p-ERK
total ERK
EGFR
HER2
Gapdh

Figure 2: mTORC1 hyperactivation in *Tsc1* cKO epidermis and keratinocytes downregulates EGFR and HER2 protein expression and activity. Immunoblotting of **(A)** WT and *Tsc1* cKO epidermal lysates, **(B)** WT and *Tsc1* cKO keratinocyte lysates and **(C)** *Tsc1* $^{flox/flox}$ keratinocyte cultures infected with empty or adenoviral cre recombinase (*Tsc1* cre) showing decreased EGFR and HER2 expression with *Tsc1* loss (left panels). Immunoblots in (B) are non-contemporaneous from the same biological replicate, while those in (C) are contemporaneous and parallel from the same biological replicate. Densitometry quantification of immunoblots (right panels) (biological replicates [r]≥4; p-values indicated are by Student's T-test). Error bars represent STDEV. **(D)** Immunoblotting following surface biotinylation and immunoprecipitation (IP) showing decreased membrane EGFR and HER2 in *Tsc1* cKO keratinocyte lysates compared to WT controls. Na-K ATPase is used to normalize for membrane protein. **(E)** Immunoblotting of WT and *Tsc1* cKO keratinocyte lysates, with or without mTORC1 inhibition using rapamycin (200 nm) or AZD8055 (500 nm), for p-S6, Tsc1, EGFR and HER2 (left panel) and p-AKT(T308), p-AKT(S473) and p-ERK (right panel). *Tsc1* cKO keratinocytes show an increase in p-S6 levels and downregulation of HER2, EGFR, p-AKT and p-ERK which were rescued upon mTORC1 inhibition. p-S6 and total S6 are non-contemporaneous immunoblots from the same biological replicate. **(F)** Immunoblotting of serum-starved, EGF-stimulated WT and *Tsc1* cKO keratinocyte lysates for EGFR, p-EGFR(Y1068), p-AKT (S473) and p-ERK. The intensity and duration of EGFR auto-phosphorylation and downstream signaling markers is decreased in *Tsc1* cKO keratinocytes.

Figure 3

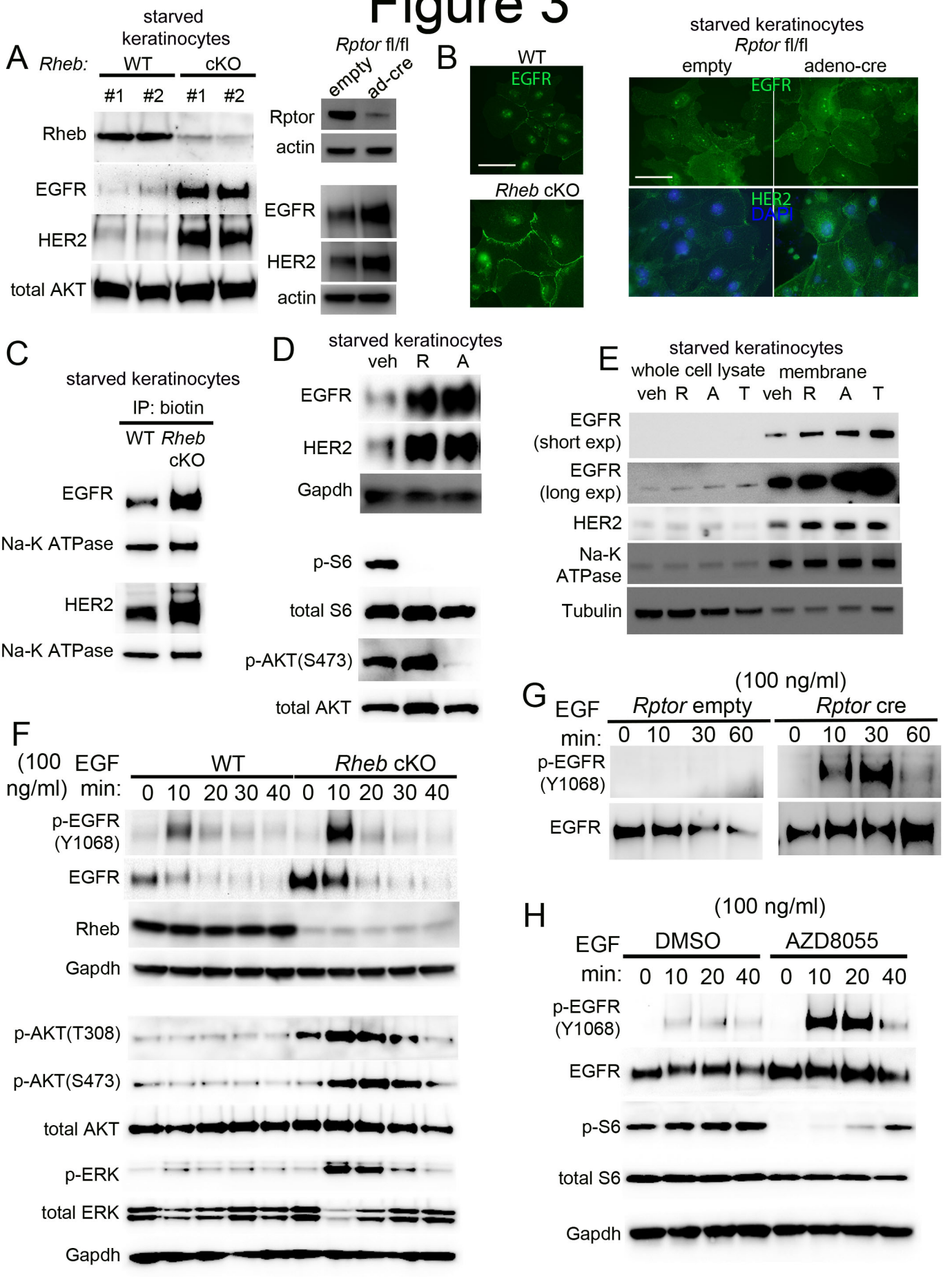
A
starved keratinocytes
Rheb:
WT
cKO
#1
#2
#1
#2
Rheb
EGFR
HER2
total AKT
Rptor fl/fl
empty
ad-cre
Rptor
actin
EGFR
HER2
actin
B
WT
EGFR
Rheb cKO
starved keratinocytes
Rptor fl/fl
empty
adeno-cre
EGFR
HER2
DAPI
C
starved keratinocytes
IP: biotin
WT
Rheb cKO
EGFR
Na-K ATPase
HER2
Na-K ATPase
D
starved keratinocytes
veh
R
A
EGFR
HER2
Gapdh
p-S6
total S6
p-AKT(S473)
total AKT
E
starved keratinocytes
whole cell lysate
membrane
veh R A T veh R A T
EGFR (short exp)
EGFR (long exp)
HER2
Na-K ATPase
Tubulin
F
(100 ng/ml)
EGF
min:
WT
Rheb cKO
0 10 20 30 40 0 10 20 30 40
p-EGFR (Y1068)
EGFR
Rheb
Gapdh
p-AKT(T308)
p-AKT(S473)
total AKT
p-ERK
total ERK
Gapdh
G
(100 ng/ml)
EGF
Rptor empty
Rptor cre
min:
0 10 30 60 0 10 30 60
p-EGFR (Y1068)
EGFR
H
(100 ng/ml)
EGF
DMSO
AZD8055
min:
0 10 20 40 0 10 20 40
p-EGFR (Y1068)
EGFR
p-S6
total S6
Gapdh

Figure 3: Genetic and pharmacological inhibition of mTORC1 up-regulates EGFR and HER2 protein expression and activity. (A) Immunoblotting showing increased expression of EGFR and HER2 in *Rheb* cKO (left panel, contemporaneous parallel immunoblots from the same biological replicate) and *Rptor* cre (right panel, Rptor and paired actin are non-contemporaneous immunoblots from the same biological replicate) keratinocyte lysates compared to WT/ empty controls respectively. **(B)** Immunofluorescence showing increased membrane EGFR (in *Rheb* cKO keratinocytes; left panels) and EGFR and HER2 (in *Rptor* cre keratinocytes; right panels) compared to WT/ empty controls respectively. Scale bar=50 μm **(C)** Immunoblotting following surface biotinylation and immunoprecipitation (IP) showing increased membrane EGFR and HER2 in *Rheb* cKO keratinocyte lysates compared to WT controls. Na-K ATPase is used to normalize for membrane protein. **(D)** Immunoblotting showing increased expression of EGFR and HER2 in rapamycin (R) or AZD8055 (A)-treated keratinocyte lysates compared to DMSO (D)-treated controls. p-S6, total S6, p-AKT and total AKT are non-contemporaneous immunoblots from the same biological replicate. **(E)** Immunoblotting following surface biotinylation and IP, showing increased membrane EGFR and HER2 in rapamycin (R), AZD8055 (A) or Torin1 (T)-treated keratinocyte lysates compared to DMSO (D) controls. Enrichment of cell surface proteins in biotin immunoprecipitates is shown using Na-K ATPase. **(F)** Immunoblotting of serum-starved, EGF-stimulated WT and *Rheb* cKO keratinocyte lysates for EGFR, p-EGFR(Y1068), p-AKT (S473), p-AKT(T308), p-ERK and Rheb. The intensity and duration of EGFR autophosphorylation and downstream signaling markers is increased in *Rheb* cKO keratinocytes. EGFR, p-EGFR(Y1068) and Rheb were immunoblotted separately using a different biological replicate. Immunoblotting of serum-starved, EGF-stimulated **(G)** empty or *Rptor* cre and **(H)** DMSO or

AZD8055-treated keratinocyte lysates for EGFR and p-EGFR(Y1068). Empty and *Rptor* cre lysates were run on the same gel, separated by a molecular weight marker.

Figure 4

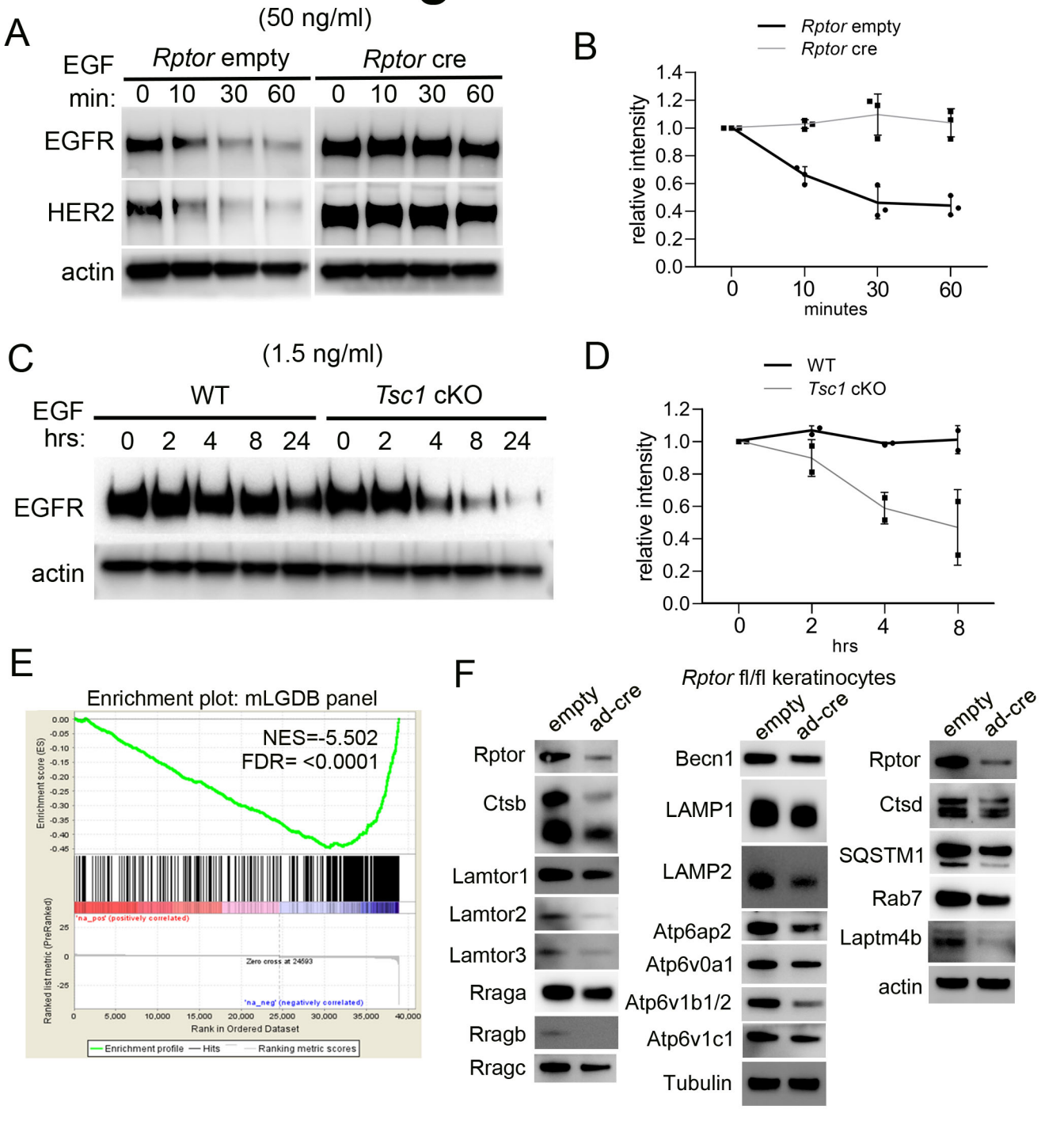
A
(50 ng/ml)
EGF
Rptor empty
Rptor cre
min: 0 10 30 60 0 10 30 60
EGFR
HER2
actin
B
Rptor empty
Rptor cre
relative intensity
minutes
C
(1.5 ng/ml)
EGF
WT
Tsc1 cKO
hrs: 0 2 4 8 24 0 2 4 8 24
EGFR
actin
D
WT
Tsc1 cKO
relative intensity
hrs
E
Enrichment plot: mLGDB panel
NES=-5.502
FDR= <0.0001
Enrichment score (ES)
'na_pos' (positively correlated)
Zero cross at 24593
'na_neg' (negatively correlated)
Ranked list metric (PreRanked)
Rank in Ordered Dataset
Enrichment profile
Hits
Ranking metric scores
F
Rptor fl/fl keratinocytes
empty
ad-cre
Rptor
Ctsb
Lamtor1
Lamtor2
Lamtor3
Rraga
Rragb
Rragc
Becn1
LAMP1
LAMP2
Atp6ap2
Atp6v0a1
Atp6v1b1/2
Atp6v1c1
Tubulin
Rptor
Ctsd
SQSTM1
Rab7
Laptm4b
actin

Figure 4: mTORC1 accelerates EGF-induced EGFR degradation. (A) Starved empty and *Rptor* cre keratinocytes were stimulated with EGF (50 ng/ml) for the indicated times and immunoblotted for EGFR. EGFR degradation curves are presented in **(B)** Error bars represent STDEV. Immunoblots are representative of three independent experiments. Empty and *Rptor* cre lysates were run on the same gel, separated by a molecular weight marker. **(C)** Starved WT and *Tsc1* cKO keratinocytes were stimulated with EGF (1.5ng/ml) for the indicated times and immunoblotted for EGFR. EGFR degradation curves are presented in **(D)** Error bars represent STDEV. Immunoblots are representative of three independent experiments. **(E)** The Gene Set Enrichment Analysis, GSEA, Enrichment Score Plot depicting the *Rptor* cKO versus *Rptor* WT fold changes of 360 lysosomal gene (from the mouse Lysosome Gene Database [mLGDB]) subset compared to those of all assayed transcripts. The green line is the Enrichment Score, reflecting the degree of lysosomal genes' overrepresentation among the *Rptor* cKO downregulated (left side) and upregulated (right side) genes. **(F)** Lysosomal proteins, including those containing a CLEAR-binding motif, are decreased in *Rptor* cre keratinocytes compared to empty controls, by immunoblot analyses. Rptor, Ctsd, SQSTM1, Rab7 Laptm4b and actin (far right panel) are non-contemporaneous immunoblots from the same biological replicate. Densitometry quantification of representative immunoblots from 4 independent experiments are provided in Figure S4A.

Figure 5

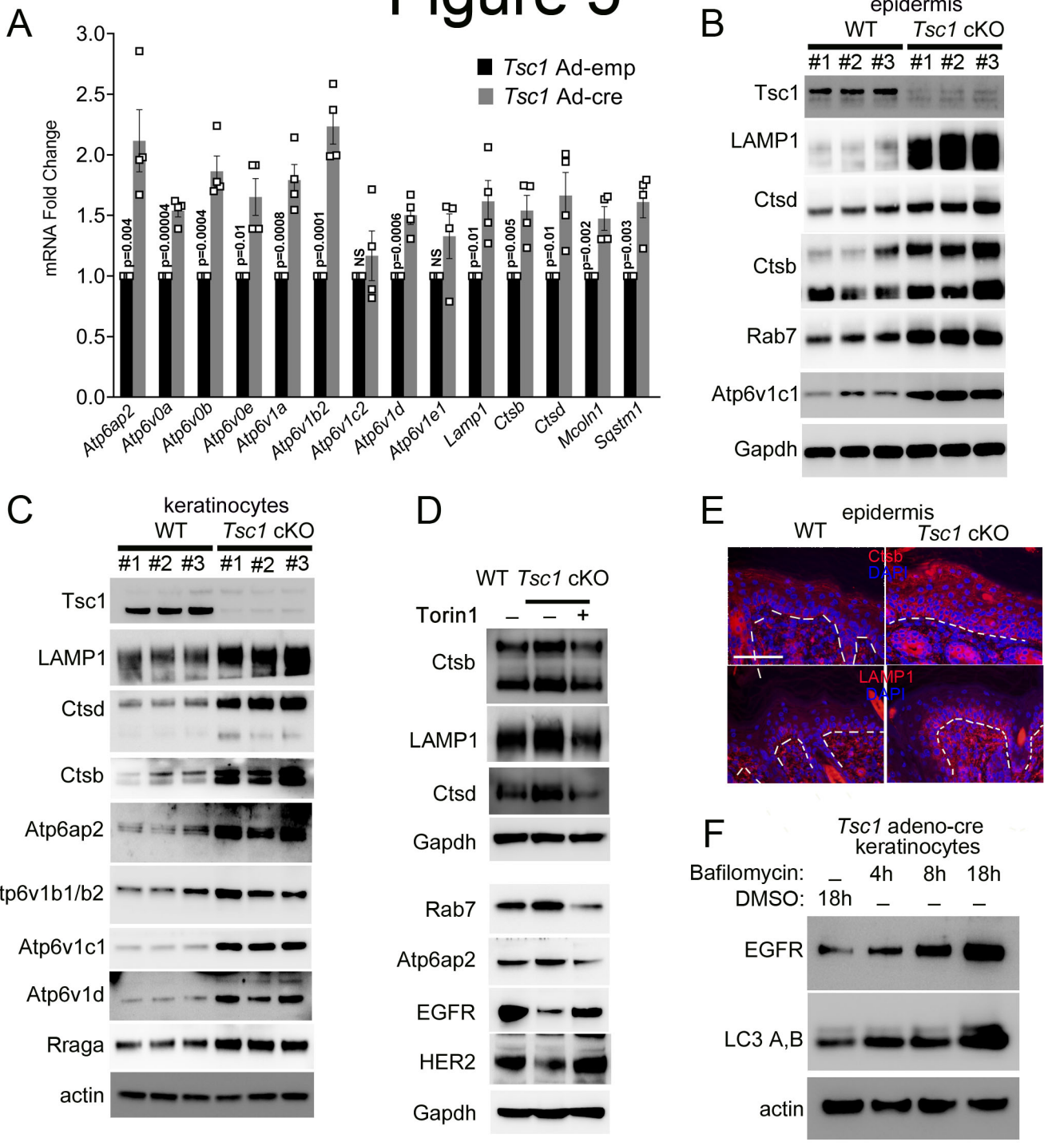
A
mRNA Fold Change
3.0
2.5
2.0
1.5
1.0
0.5
0.0
Tsc1 Ad-emp
Tsc1 Ad-cre
p=0.004
p=0.00004
p=0.0004
p=0.01
p=0.0008
p=0.0001
NS
p=0.0006
NS
p=0.01
p=0.005
p=0.01
p=0.002
p=0.003
Atp6ap2
Atp6v0a
Atp6v0b
Atp6v0e
Atp6v1a
Atp6v1b2
Atp6v1c2
Atp6v1d
Atp6v1e1
Lamp1
Ctsb
Ctsd
Mcoln1
Sqstm1
B
epidermis
WT
Tsc1 cKO
#1 #2 #3 #1 #2 #3
Tsc1
LAMP1
Ctsd
Ctsb
Rab7
Atp6v1c1
Gapdh
C
keratinocytes
WT
Tsc1 cKO
#1 #2 #3 #1 #2 #3
Tsc1
LAMP1
Ctsd
Ctsb
Atp6ap2
Atp6v1b1/b2
Atp6v1c1
Atp6v1d
Rraga
actin
D
WT Tsc1 cKO
Torin1 – – +
Ctsb
LAMP1
Ctsd
Gapdh
Rab7
Atp6ap2
EGFR
HER2
Gapdh
E
epidermis
WT
Tsc1 cKO
Ctsb
DAPI
LAMP1
DAPI
F
Tsc1 adeno-cre
keratinocytes
Bafilomycin: – 4h 8h 18h
DMSO: 18h – – –
EGFR
LC3 A,B
actin

Figure 5: mTORC1 activates lysosomal gene expression. (A) Quantitative real time PCR (qRT-PCR) showing up-regulation of lysosomal CLEAR target gene transcripts in *Tsc1* cre keratinocytes compared to empty controls (r=4, error bars represent SEM; p values are by Student's t-test). Expression of lysosomal CLEAR gene targets is increased in *Tsc1* cKO epidermis **(B)** and *Tsc1* cKO keratinocytes **(C)**, compared to WT controls, by immunoblot analyses. **(D)** Expression of lysosomal proteins is increased in *Tsc1* cKO keratinocytes compared to empty controls, and is downregulated in response to Torin1 (1μM, 24 hrs), by immunoblot analyses. Ctsb, LAMP1 and Ctsd were immunoblotted separately using a different biological replicate. **(E)** Immunostaining for Ctsb and LAMP1 showing expansion of the lysosomal compartment in basal keratinocytes of *Tsc1* cKO epidermis compared to WT controls; white lines demarcate dermal-epidermal junction. Scale bar=150 μm. **(F)** *Tsc1* cre keratinocytes treated with the lysosomal V-ATPase inhibitor Bafilomycin A1 (100nm), rescued EGFR expression in a time-dependent manner.

Figure 6

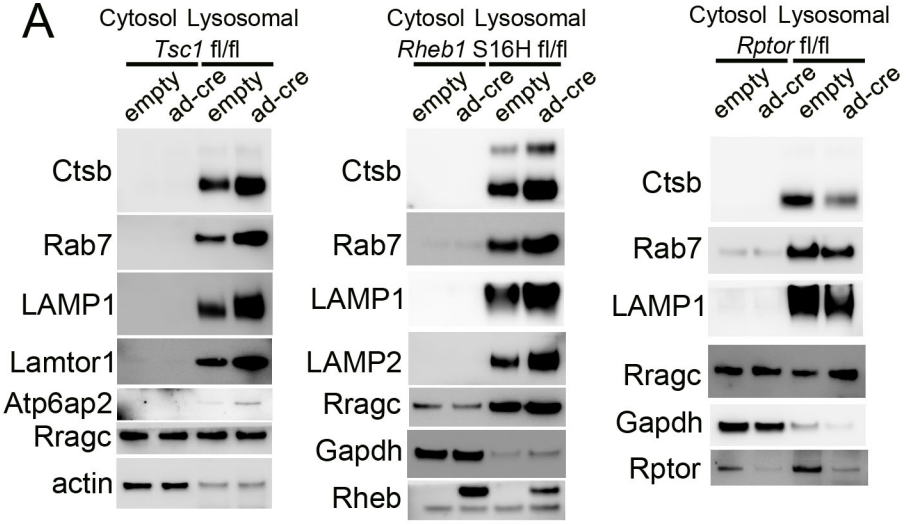
A
Cytosol Lysosomal
Tsc1 fl/fl
empty
ad-cre
empty
ad-cre
Ctsb
Rab7
LAMP1
Lamtor1
Atp6ap2
Rragc
actin
Cytosol Lysosomal
Rheb1 S16H fl/fl
empty
ad-cre
empty
ad-cre
Ctsb
Rab7
LAMP1
LAMP2
Rragc
Gapdh
Rheb
Cytosol Lysosomal
Rptor fl/fl
empty
ad-cre
empty
ad-cre
Ctsb
Rab7
LAMP1
Rragc
Gapdh
Rptor

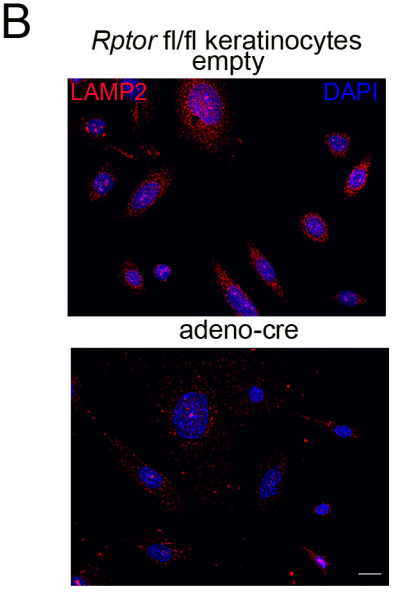
B
Rptor fl/fl keratinocytes
empty
LAMP2
DAPI
adeno-cre

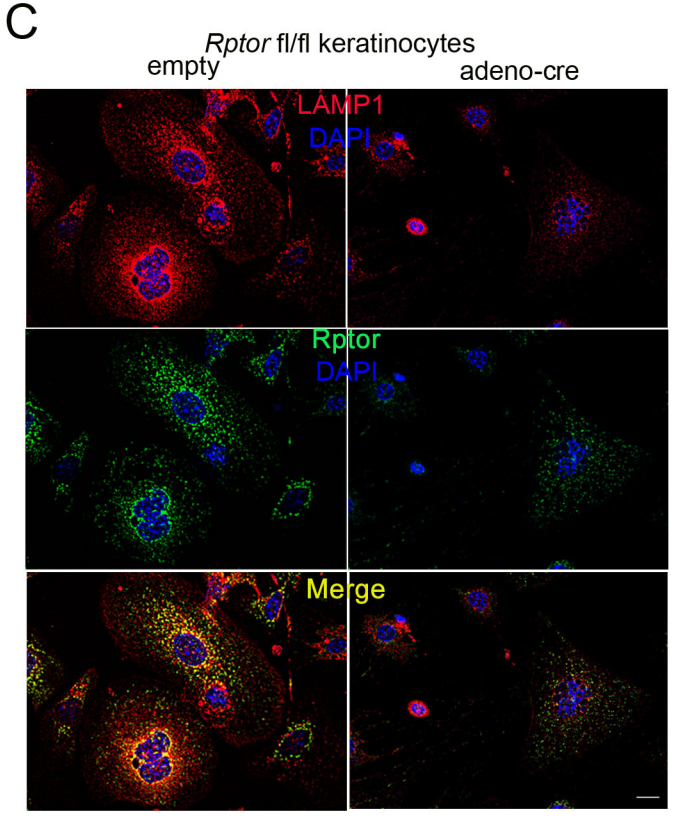
C
Rptor fl/fl keratinocytes
empty
adeno-cre
LAMP1
DAPI
Rptor
DAPI
Merge

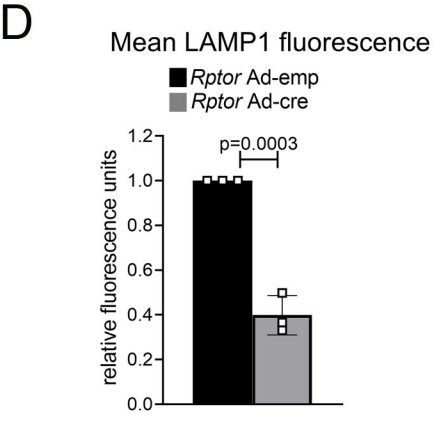
D
Mean LAMP1 fluorescence
Rptor Ad-emp
Rptor Ad-cre
p=0.0003
relative fluorescence units
1.2
1.0
0.8
0.6
0.4
0.2
0.0

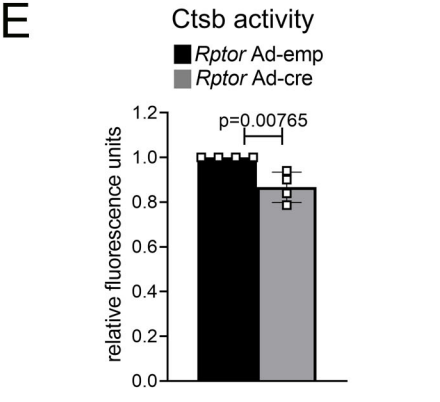
E
Ctsb activity
Rptor Ad-emp
Rptor Ad-cre
p=0.00765
relative fluorescence units
1.2
1.0
0.8
0.6
0.4
0.2
0.0

Figure 6: mTORC1 promotes lysosomal biogenesis and activity. (A) Immunoblot analyses of lysosomal proteins in lysosomal fractions of cellular lysates, showing increased expression of lysosomal proteins in *Tsc1* cre keratinocytes (left panel) and *Rheb1* S16H Tg keratinocytes (middle panel) compared to controls, and decreased expression of lysosomal proteins in *Rptor* cre keratinocytes (right panel) compared to controls. Lysosomal marker Rragc was unaltered across genotypes and used as a loading control. **(B)** Confocal microscopy analyses of LAMP2 immunostaining demonstrates decreased presence of LAMP2 in *Rptor* cre keratinocytes compared to empty controls. Scale bar=100μm **(C)** Confocal microscopy analyses and double immunostaining for LAMP1/Rptor demonstrates decreased presence of Lamp1 and Rptor in *Rptor* cre keratinocytes compared to empty controls. Scale bar= 100μm **(D)** Quantification of LAMP1 fluorescence intensity showing a decrease in mean LAMP1 fluorescence in *Rptor* cre keratinocytes compared to controls. The area of LAMP1 was measured using Image J and normalized to the number of nuclei. (r=3, n>1000). Error bars represent STDEV, p=0.0003 by Student's t-test. **(E)** Lysosomal activity, as measured by fluorometric analyses of cathepsin B activity using the Magic Red Cathepsin B kit is decreased in *Rptor* cre keratinocytes compared to controls (r=4, error bars represent STDEV; p= 0.007 by Student's t-test).

Figure 7

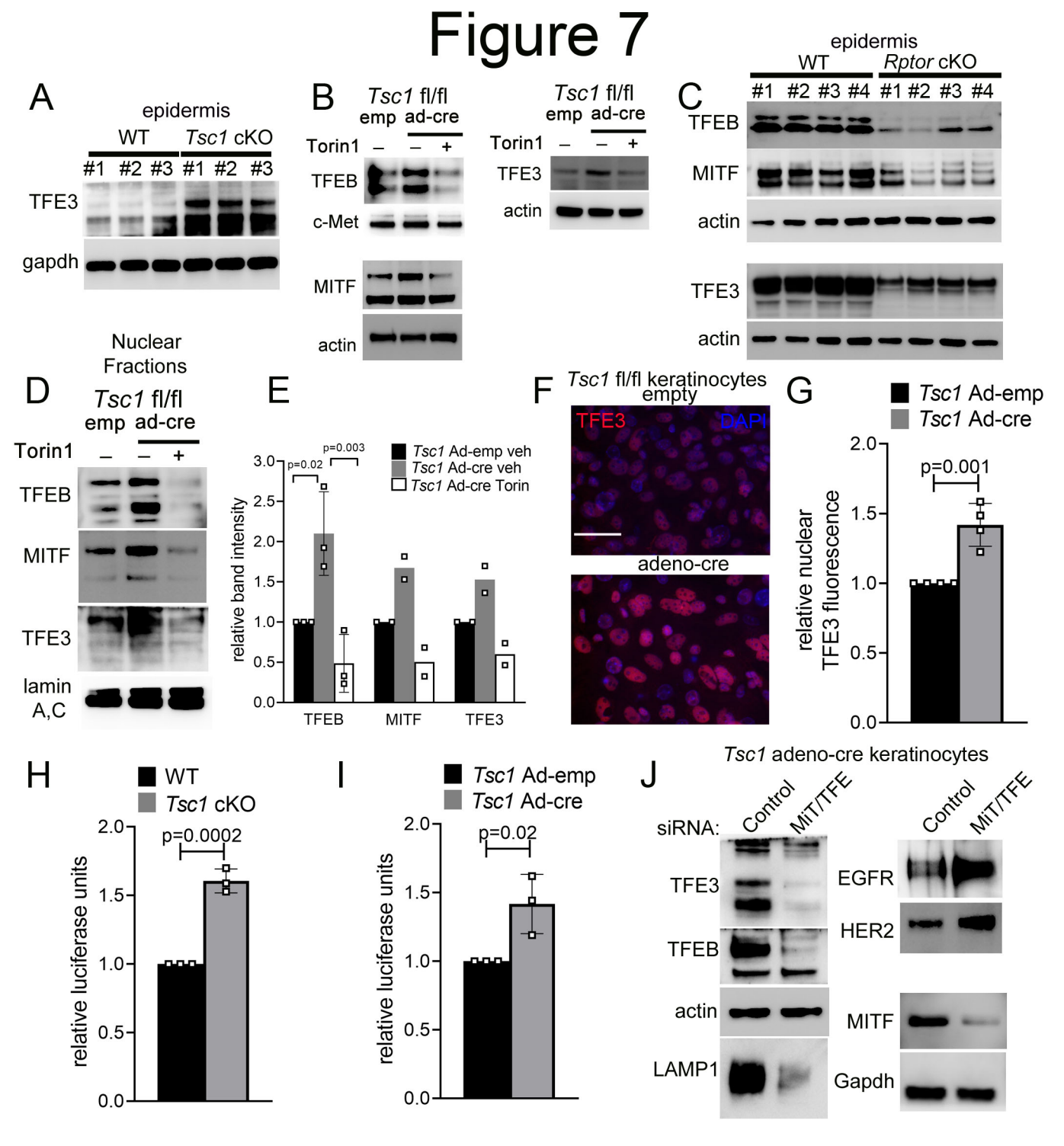
A
epidermis
WT
Tsc1 cKO
#1 #2 #3 #1 #2 #3
TFE3
gapdh
B
Tsc1 fl/fl
emp ad-cre
Torin1 – – +
TFEB
c-Met
MITF
actin
Tsc1 fl/fl
emp ad-cre
Torin1 – – +
TFE3
actin
C
epidermis
WT
Rptor cKO
#1 #2 #3 #4 #1 #2 #3 #4
TFEB
MITF
actin
TFE3
actin
D
Nuclear Fractions
Tsc1 fl/fl
emp ad-cre
Torin1 – – +
TFEB
MITF
TFE3
lamin A,C
E
p=0.02
p=0.003
Tsc1 Ad-emp veh
Tsc1 Ad-cre veh
Tsc1 Ad-cre Torin
relative band intensity
3.0
2.5
2.0
1.5
1.0
0.5
0.0
TFEB
MITF
TFE3
F
Tsc1 fl/fl keratinocytes
empty
TFE3
DAPI
adeno-cre
G
Tsc1 Ad-emp
Tsc1 Ad-cre
p=0.001
relative nuclear TFE3 fluorescence
2.0
1.5
1.0
0.5
0.0
H
WT
Tsc1 cKO
p=0.0002
relative luciferase units
2.0
1.5
1.0
0.5
0.0
I
Tsc1 Ad-emp
Tsc1 Ad-cre
p=0.02
relative luciferase units
2.0
1.5
1.0
0.5
0.0
J
Tsc1 adeno-cre keratinocytes
siRNA:
Control
MiT/TFE
TFE3
TFEB
actin
LAMP1
Control
MiT/TFE
EGFR
HER2
MITF
Gapdh

Figure 7: mTORC1 drives MiT/TFE expression, nuclear localization and CLEAR promoter activity. (A) Immunoblotting showing increased expression of MiT/TFE proteins in *Tsc1* cKO epidermal lysates and represent the same experiment as depicted as in Figure 5B. **(B)** Immunoblotting showing increased expression of MiT/TFE proteins in *Tsc1* cre keratinocytes compared to controls, and decreased expression in response to Torin1 (1μM, 24 hrs). TFEB and paired c-Met as well as MITF and paired actin represent contemporaneous parallel immunoblots from the same biological replicate. TFE3 and paired actin were immunoblotted separately using a different biological replicate. **(C)** Immunoblotting showing decreased expression of MiT/TFE proteins in *Rptor* cKO epidermal lysates compared to controls. TFE3 was immunoblotted separately using different biological replicates. **(D)** MiT/TFE proteins are increased in nuclear-fraction immunoblots of *Tsc1* cre keratinocytes compared to controls, and downregulation in response to Torin1 (1μM, 24 hrs). Lamin A/C is used to normalize for nuclear protein. These are contemporaneous parallel immunoblots from the same biological replicate. **(E)** Densitometry quantification of representative immunoblot experiments shown in (D), ($r \geq 2$; error bars represent STDEV; p-values by one-way ANOVA). **(F)** Immunofluorescence showing increased nuclear localization of TFE3 in *Tsc1* cre keratinocytes, compared to controls. (left panel; Scale bar=150 μm). **(G)** Quantification of nuclear TFE3 fluorescence from experiments in (F) ($r=4$; $n > 1293$; $p=0.001$ by Student's T-test). 4X-CLEAR luciferase reporter activity at 48 hrs is: **(H)** increased in *Tsc1* cKO and **(I)** *Tsc1* cre keratinocytes, compared to controls. Renilla is used to normalize for luciferase activity. ($r=3$; error bars represent STDEV; p-values by Student's T-test). **(J)** *Tsc1* cre keratinocytes transfected with TFEB, TFE3 and MiTF siRNA show increased EGFR and HER2 expression, compared to negative control siRNA, by immunoblot analyses. MITF was immunoblotted separately using the same biological replicate.

Figure 8

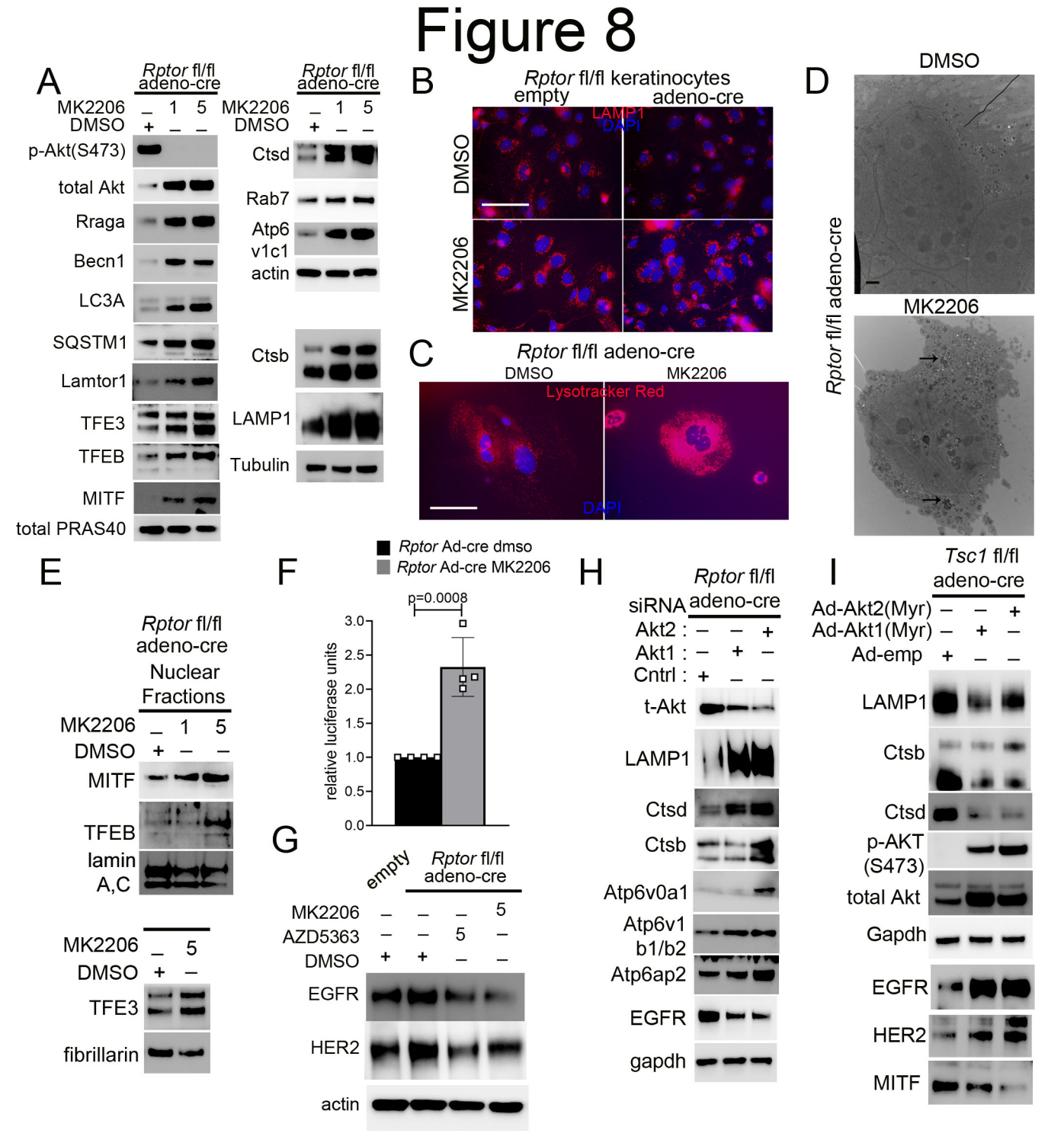
A
Rptor fl/fl adeno-cre
MK2206 – 1 5
DMSO + – –
p-Akt(S473)
total Akt
Rraga
Becn1
LC3A
SQSTM1
Lamtor1
TFE3
TFEB
MITF
total PRAS40
Rptor fl/fl adeno-cre
MK2206 – 1 5
DMSO + – –
Ctsd
Rab7
Atp6 v1c1
actin
Ctsb
LAMP1
Tubulin
B
Rptor fl/fl keratinocytes
empty
adeno-cre
LAMP1
DAPI
DMSO
MK2206
C
Rptor fl/fl adeno-cre
DMSO
MK2206
Lysotracker Red
DAPI
D
DMSO
MK2206
Rptor fl/fl adeno-cre
E
Rptor fl/fl adeno-cre
Nuclear Fractions
MK2206 – 1 5
DMSO + – –
MITF
TFEB
lamin A,C
MK2206 – 5
DMSO + –
TFE3
fibrillarin
F
Rptor Ad-cre dmso
Rptor Ad-cre MK2206
p=0.0008
relative luciferase units
3.0
2.5
2.0
1.5
1.0
0.5
0.0
G
empty
Rptor fl/fl adeno-cre
MK2206 – – – 5
AZD5363 – – 5 –
DMSO + + – –
EGFR
HER2
actin
H
Rptor fl/fl adeno-cre
siRNA
Akt2 : – – +
Akt1 : – + –
Cntrl : + – –
t-Akt
LAMP1
Ctsd
Ctsb
Atp6v0a1
Atp6v1 b1/b2
Atp6ap2
EGFR
gapdh
I
Tsc1 fl/fl adeno-cre
Ad-Akt2(Myr) – – +
Ad-Akt1(Myr) – + –
Ad-emp + – –
LAMP1
Ctsb
Ctsd
p-AKT (S473)
total Akt
Gapdh
EGFR
HER2
MITF

Figure 8: Inhibition of hyperactive AKT in mTORC1-inhibited cells rescues autophagy/ lysosomal biogenesis and downregulates EGFR expression. (A) Immunoblotting showing increased expression of lysosomal, autophagy and MiT/TFE proteins in *Rptor* cre keratinocytes treated with MK2206 (1, 5μM; 8hrs). Ctsb, LAMP1 and tubulin are non-contemporaneous immunoblots of the same biological replicate, while all other blots are contemporaneous parallel immunoblots of the same biological replicate. **(B)** LAMP1 immunostaining showing expansion and perinuclear localization of lysosomes in empty and *Rptor* cre keratinocytes treated with MK2206 (5μM, 8hrs), compared to DMSO controls. Scale bar=50 μm. **(C)** MK2206-treated *Rptor* cre keratinocytes show increased LysoTracker Red fluorescence compared to DMSO controls**.** Scale bar=40 μm. **(D)** Electron micrographs showing increased presence of autophagic vesicles (black arrows) in MK2206-treated *Rptor* cre keratinocytes, compared to DMSO controls. Scale bar=2 μm. **(E)** MiT/TFE proteins are increased in nuclear-fraction immunoblots of MK2206-treated *Rptor* cre keratinocytes (1, 5μM; 8hrs). Lamin A/C and Fibrillarin are used as loading controls. **(F)** MK2206 treatment of *Rptor* cre keratinocytes increases 4X-CLEAR luciferase reporter activity. Renilla is used to normalize for luciferase activity. (r=4; error bars represent STDEV; p-values by Student's T-test). **(G)** Immunoblotting showing decreased expression of EGFR and HER2 in *Rptor* cre keratinocytes treated with MK2206/AZD5363 for 24hs. **(H)** Immunoblotting showing increased expression of lysosomal markers and MiT/TFE proteins with downregulation of EGFR expression in *Rptor* cre keratinocytes treated with AKT1/2 siRNA. **(I)** Immunoblotting showing decreased expression of lysosomal markers and MiT/TFE proteins with upregulation of EGFR and HER2 expression in *Tsc1* cre keratinocytes infected with (Myr-AKT1) or (Myr-AKT2) adenovirus.